Pre-normative REsearch for Safe use of Liquid Hydrogen (PRESLHY)

Project Deliverable

Experimental investigation of cryogenic hydrogen release and mixing

Deliverable Number:	3.3 (D20)
Work Package:	3
Version:	1.0
Author(s), Institution(s):	T. Jordan, KIT
Submission Date:	31 May 2021
Due Date:	31 May 2021
Report Classification:	Public

FUEL CELLS AND HYDROGEN
JOINT UNDERTAKING

This project has received funding from the Fuel Cells and Hydrogen 2 Joint Undertaking under the European Union's Horizon 2020 research and innovation programme under grant agreement No 779613.

History		
Nr.	Date	Changes/Author
1.0	31.5.2021	Release version by T. Jordan KIT

Approvals			
Version	Name	Organisation	Date
-			

Acknowledgements

This project has received funding from the Fuel Cells and Hydrogen 2 Joint Undertaking under the European Union's Horizon 2020 research and innovation programme under grant agreement No 779613.

Disclaimer

The data management in the PRESLHY project follows the principle of data management, which shall make data Findable, Accessible, Interoperable and Re-usable (FAIR). The plan for FAIR data management as described in this document is based on the corresponding template for open research data management plan (DMP) of the European Research Council (ERC).

Despite the care that was taken while preparing this document the following disclaimer applies: The information in this document is provided as is and no guarantee or warranty is given that the information is fit for any particular purpose. The user thereof employs the information at his/her sole risk and liability.

The document reflects only the authors' views. The FCH JU and the European Union are not liable for any use that may be made of the information contained therein.

Key Words

Cryogenic release, high pressure, discharge coefficient, jet dispersion, electrostatic field, far field observation, mixing, LH2, pool, evaporation, rain-out

Publishable Short Summary

Within the experimental program of PRESLHY 4 experimental campaigns address the non-reactive phenomena release and mixing. The DISCHA experimental campaign (E3.1a) consisted of more than 200 hydrogen high pressure blow-down experiments applying the DISCHA-facility at KIT. About half of the experiments were made at cryogenic temperatures (approx. 80 K). With the new built CRYOSTAT facility of KIT 12 similar hydrogen blow-down experiments were performed with LH2 (E3.1b). Not a single test showed a spontaneous ignition, although at least the cold high pressure jets generated relative strong electrostatic fields. This static electricity seems to be generated by ice crystals which form on the release nozzle before the tests and are broken and entrained when the discharge is initiated.

With the POOL experiments (E3.4) at KIT the influence of ground materials and side wind on the evaporation rates of LH2 was assessed. Four different ground materials were tested: concrete, sand, gravel and water. The results were used to validate corresponding models. The gravel material caused highest evaporation rate and accordingly largest flammable mixtures above the pools.

The RAINOUT experiments (E3.5) of HSE demonstrated the little potential for rain-out and pool formation even at massive release rates. Field measurements for concentration and temperature measurement revealed a useful correlation for cryogenic releases. Similar as for the DISCHA experiments the generated electrical fields and currents turned out to be too small to represent a credible ignition source.

Table of Contents

1 Overview on Release and Mixing Experiments

The general objective of WP3 was to close knowledge gaps, develop and validate suitable models for phenomena relevant to the non-reactive accidental phase, release and mixing of liquid hydrogen (LH2), cryogenic hydrogen respectively. For the most relevant, highly prioritised phenomena new high quality validation data should be generated experimentally to allow developing new models and engineering correlations, applicable for corresponding hazard, risk or safety assessments.

The addressed phenomena included, but were not limited to

- Flashing multiphase, multicomponent release phenomena
- Mass and heat transfer including phase transition (evaporation, condensation and freezing of contaminants) in pools, plumes, jets and sprays
- Free cryogenic jet principle structure, morphology and behaviour in realistic conditions including flammable envelope
- Heat transfer effect on hydrogen concentration in impinging and/or wall attached jets
- Effect of wind speed and direction on large-scale LH2 releases
- Release and dispersion in confined and obstructed spaces, including pressure-peaking phenomena.

This initial list was translated in an initial set of proposed tests, which was deemed to be possible with the limited funding. Table 1 shows this set initially program suggested, which contained also optional experiments (in *italic*) for multi-phase high pressure and mid-scale experiments. Those optional experiments were suggested for cases where industry partners might invest in extra work or if in a later phase a planned test series would turn out to be impractical to execute.

The actual experimental program was refined after the initial PIRT exercise (Deliverable D2.5 www.preslhy.eu/deliverables) and the research priorities workshop (Deliverable D2.4) organised by work package WP2. Finally, the experimental work in work package WP3 of PRESLHY, addressing the non-reactive initiating phase of prototypical accidents consisted of 4 experimental campaigns (see Table 2).

Table 1: Original table of release and mixing experiments with optional tests in italic

WP/ Exp. Nr.	Phenomena/ Name	Issue addressed/ Objective	To be investigated	Variation of	Range of variables	n of variations	Partner/ Test facility
WP3	**Release and Mixing**						
E3.1	**Small Scale Multi-phase Release**	Discharge Coefficients of Pressurized or LH2 Releases	pressure changes in bulk vessel temperature changes in a jet mass flow rate inertia (thrust), weight BOS images, laser diagnostics of jet principle structure, potential wall attachment/ impingement	Initial pressure Initial temperature Nozzle shape and cross-sectional area Extraction point (high/gaseous-low/liquid & middle)	0-200 bar (sub-critical & supercritical) 25-200K	4 4 4 3	KIT/ HYKA-H8(He) DISCHA-facility in Test chamber V = 2.867 dm³
E3.2	***Multi-phase High Pressure Release***	*Charcterisation of Pressurised LH2 releases using characteristic pipe diameters* *Scale up of E3.1 wrt inventory, release rates & p*		*Pressure, temperature, release type (length and diameter, orientation, thrust, discharge coefficient*	*0-1000 bar? (or highest pressure possible)*	*t.b.d.*	*HSL/ Suitable vessel required/system required*
E3.3	***Mid-Scale Multi-phase Release***	*LH2 jets/near field cloud dispersion*	*flash rate, momentum, velocity (Temperature pressure and concentration measurements in the near field from 0 to 1m), Cloud dispersion : temperature et concentration measurements (field instrumentation ~10 m)*	*orifice size , pressure*	*5/15 mm ; 0-10bar*	*3 x 3*	*INERIS/ 2 m3 vessel + 20 m line (1"ID)+discharge valve+calibrated orifice*
E3.4	**Pool of LH2**	Evaporation a spill of LH2 1 m2	evaporation rate, cold gas mixing, O2 entrainment BOS imaging temperature profile in a gas concentr. profile in a gas	Material of the ground Initial temperature	solid-liquid-porous 77-300K	3 3	KIT/ HYKA-H110(N2)
E3.5	**Rainout Tests**	LH2 Spray evaporation/ Pool formation	evaporation rate, pool formation		release height release up/down/ horizont.	3 3	HSL/ Pool facility

In the experimental campaign E3.1a small scale multi-phase discharges were studied by the partners KIT and Pro-Science. The DISCHA facility was used for these tests, which allowed for pressures up to 20 MPa and temperatures down to 77 K. For lower temperatures down to 20 K a special facility, the CRYOSTAT facility was constructed by the same partners. Thus discharges directly from LH2 could be studied in the experimental series E3.1b. However, the pressure was limited to 0.5 MPa for these tests. In the campaign E3.4 the release from small scaled pools filled with LH2 was studied again by KIT and Pro-Science. The influence of four different substrates for simulating different ground materials and of different side wind conditions on the evaporation behaviour was investigated.

The only large scale experiments in PRESLHY are constituted by the E3.5 rainout tests done by HSE. Release of large inventories (close to trailer relevant quantities) through large diameters. Concentration field measurements and the principle chance for observing rain-out in dependence of release height and direction were checked.

The small scale DISCHA and the rain-out experiments were additionally used to quantify electrostatic field and electric current generation during the discharges. These measurements are formally attributed to work package WP4, dealing with ignition phenomena.

Table 2: Executed experimental program for release and mixing

EXP. NR.	Phenomena	To be investigated	In facility of	Variation of	Deliverable Links, References
E3.1a	Small Scale Cryogenic Release	Change of state (p,T) in the pressure reservoir. Discharge coefficients. External jet principle structure and multiphase effects	DISCHA, KIT	Initial pressure 0.5-20 MPa Initial temperature 80 K and 300 K Nozzle cross-sectional area	D3.4 bwdatadiss.kit.edu/dataset/179
E3.1b	Small Scale Multi-phase Release	Change of state (p,T) in cryostat Discharge rates bulk vessel BOS images of jet principle structure including multiphase effects	CRYOSTAT, KIT	Temperature; Nozzle cross-sectional area; Extraction point (high/gaseous-low/liquid & middle)	D3.4 bwdatadiss.kit.edu/dataset/
E3.4	Small Pools of LH2	Evaporation rate Cold gas mixing and O2 entrainment profile in a gas	POOL, KIT	Material of the ground; Initial temperature; Cross-wind	D3.5 bwdatadiss.kit.edu/dataset/
E3.5	Large Scale Rainout Tests	Evaporation rate, pool formation, external mixing and field measurements of concentration and T under different weather conditions	Spill platform HSE	Diameter, height above ground and orientation of release orifice	D3.6 bwdatadiss.kit.edu/dataset/

In the following the four test campaigns are described in more detail.

2 DISCHA Experiments E3.1a

In these experiments the modified DISCHA facility was applied by KIT and Pro-Science to investigate releases of cryogenic hydrogen at temperatures of approximately 80 K and pressures up to 20 MPa. For comparison similar releases were performed with the pressure reservoir at ambient temperature. So actually two experimental series, one reference test series at ambient temperature and the other using a liquid nitrogen (LN2) pool for cooling, were performed with the DISCHA facility.

The main purpose of the tests was to provide validation or reference data for

- models defining or using a discharge coefficient,
- subsequent explosion tests, where the released gases are ignited forming transient jet fires or fire balls (see test series E5.2), and
- electrostatic field excitation and associated ignition potential of high pressure hydrogen gas jets at cryogenic temperatures.

2.1 General description of the DISCHA facility

The DISCHA facility mainly consists of a stainless-steel pressure vessel with an internal free volume of 2.815 dm³ and a weight of about 28 kg, which is fastened in an insulated box for the LN_2 pool cooling. A sketch of the facility are shown Figure 1.

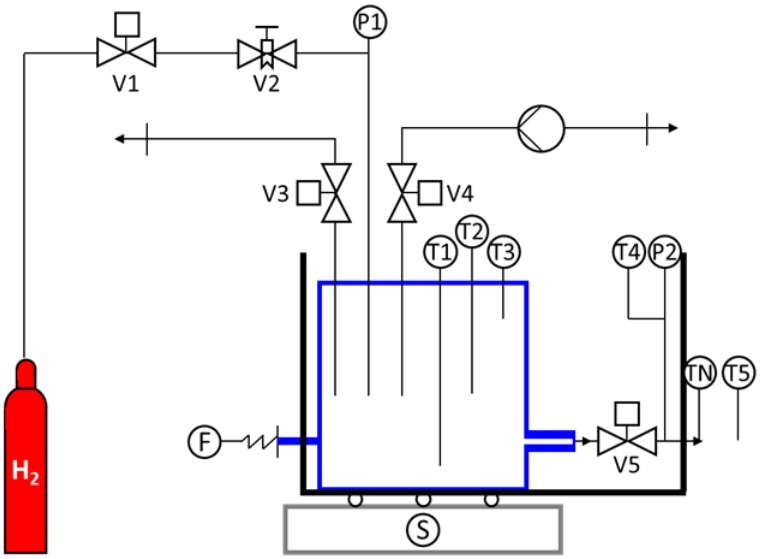

Figure 1: Sketch of the DISCHA facility
(DISCHA in blue color, cooling box in bold black color, balance in grey color).

The cooling box with the vessel is mounted on a sledge and this sledge is mounted on a high precision balance. The total weight of the experimental set-up, as measured by the balance is about 120 kg. Photographs of the facility and a sketch of the facility are shown in Figure 2.

Figure 2: Photographs of the DISCHA -pressure vessel (left) and the general set-up of the DISCHA-facility (right).

Through the filling line and the valves V1 and V2 the test vessel can be filled with hydrogen up to pressures of 20 MPa from a bundle of hydrogen bottles (see Figure 1).

The vessel is equipped with several ports for instrumentation on its top and a rod that points on a force sensor on its rear side. Opposite to the force sensor a tubular exhaust pipe is welded to the vessel, where release nozzles with different aperture sizes, nozzle diameters respectively, can be fastened. The sledge provides an almost slip free movement of the setup for the measurement of the repulsive forces, that act on the vessel during the release experiments. The balance is used to measure the loss of weight caused by the effusing hydrogen.

Four nozzles with circular apertures of 0.5, 1, 2 and 4 mm were used in the experiments. The nozzles were mounted from outside the pool to the tube that connects them to the release valve (see **Fehler! Verweisquelle konnte nicht gefunden werden.**). Another connection, which is kept as short as possible, is mounted in between the release valve and the vessel exhaust

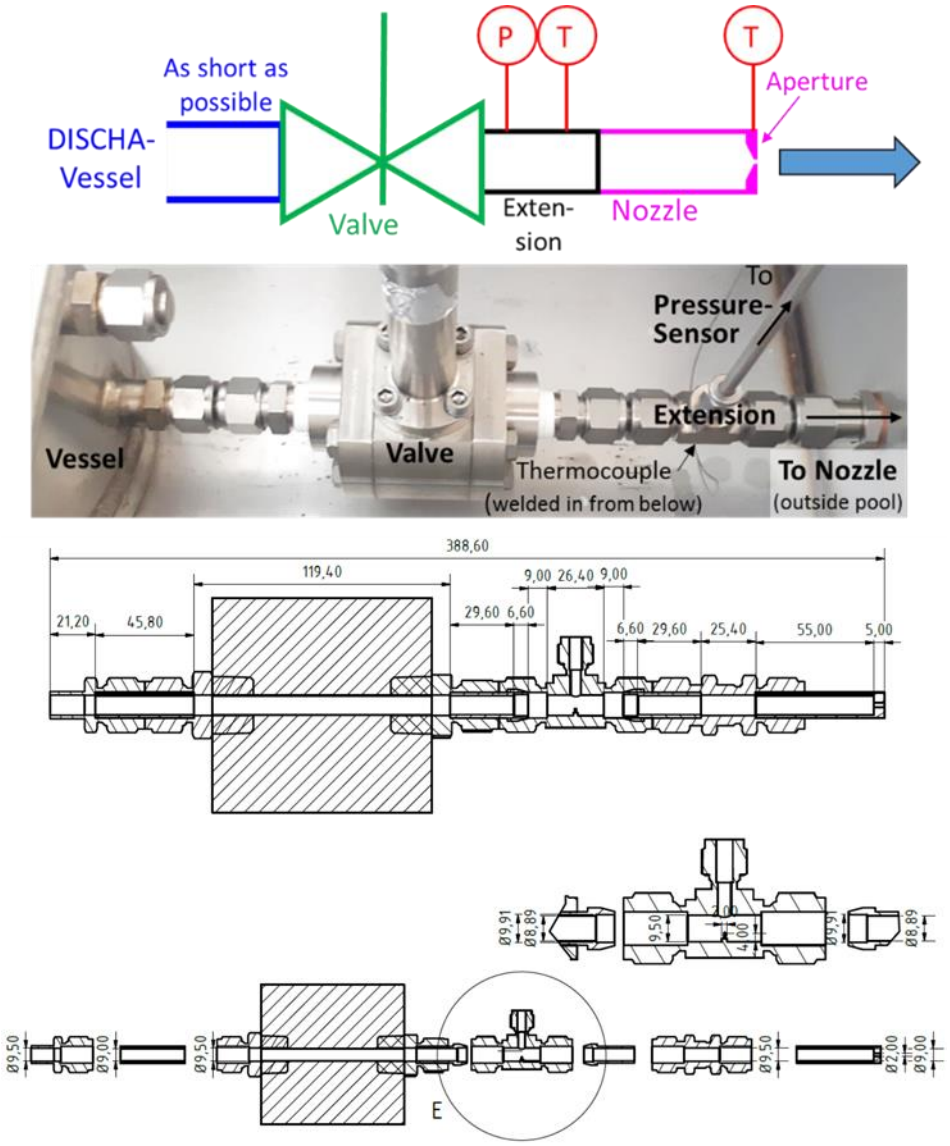

Figure 3: Sketch, photo and technical drawing of the release pipework of the DISCHA-facility with the 2 mm release nozzle (only diameter Ø 2 is changed for other nozzles).

In pre-tests, the opening-time of the valve was determined by high speed video recording (240 fps) of the indicator disc at the top of the valve head. In the background of the indicator disc an optical clock was positioned that uses LED-bars in a binary logic for indicating the time span that has elapsed after the trigger signal was issued. The disc is directly connected to the ball inside the ball valve and thus accurately indicates the degree of valve opening. From the pre-tests a valve-delay time of 40 ms is determined, after which the valve shows its first movement. During the following 180 ms the valve then opens completely.

2.2 Instrumentation of the DISCHA facility

Apart from the force sensor (Althen, Type ALF318CPR0K0, 0 - 2 kN) and the balance (Mettler-Toledo, PBA430x, 0 - 150 kg, F and S, see Figure 2 right), the test vessel and the release nozzle are instrumented with two pressure sensors and eight thermocouples. Outside the release nozzle further five thermocouples and a set of five H_2-concentration measurement devices are installed. Additionally, two electric fieldmills for measuring

static electric field strength. Three cameras (2 photo cameras and 1 video camera) are used to monitor the external mixing process using the BOS-technique for the visualization of density gradients.

Pressure sensors: One static pressure sensor (P1 in Figure 1) in the filling line is used to control the initial pressure inside the vessel during the filling procedure, while the second one measures the pressure changes in the release line. Since the second sensor is connected to the tube in between release valve and nozzle, the first increase in this signal corresponds to the actual start of the release. After the initial pressure built-up in the release line both pressure sensors capture the pressure decrease inside the vessel during the experiment.

Thermocouples (TCs): Three sets of NiCr/Ni-thermocouples (Type K) are used in the DISCHA facility. Two sets (three TCs each) are installed inside the vessel to record the gas temperature during the experiment in different heights. The sensor arrangement is used to check the accuracy and the rise time of the three standard TCs (T1 to T3, diameter 0.36 mm, sensitive tip covered by thin stainless steel shell) with a second set of three very thin open TCs (T1o to T3o, diameter 0.25 mm, stainless steel shell of sensitive tip removed). Both sets are installed in comparable positions inside the vessel. In the release line two further standard TCs are positioned: T4 is welded into the line to measure the temperature inside, while TN is mounted from the outside in a hole in the material of the stainless steel nozzle aperture with no direct contact to the released gas. Five standard TCs are distributed outside the release nozzle in the mixing domain. Three of these (T5 to T7) are located in distances of 250 mm, 750 mm and 1750 mm from the nozzle on its centerline, while T8 and T9 are positioned in distances of 250 mm and 500 mm slightly to the right and to the left of the nozzle centerline (see **Fehler! Verweisquelle konnte nicht gefunden werden.**).

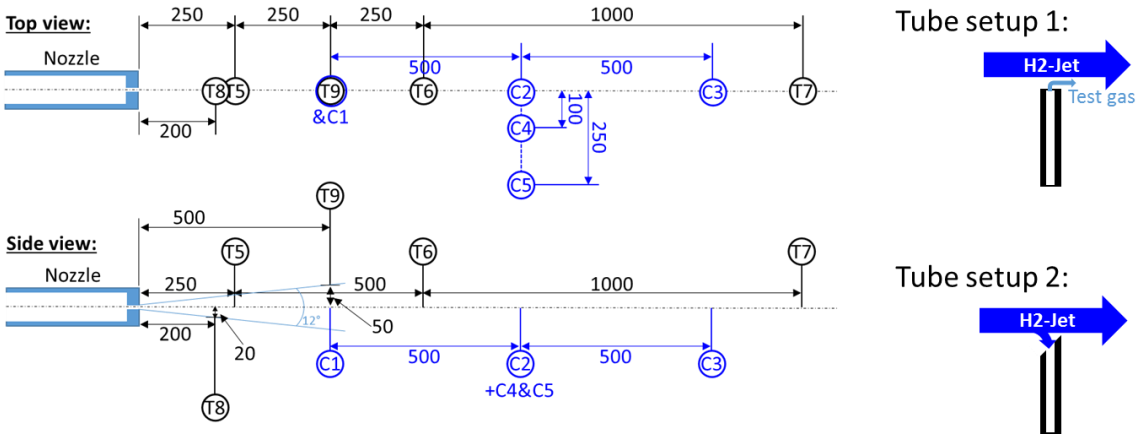

Figure 4: Sketches of the ex-vessel instrumentation of the DISCHA-facility and configurations of the plastic tubes for the H_2-concentration measurements.

Concentration measurements: Five Messkonzept H_2-sensors are utilized to determine the hydrogen concentration in different positions in the free hydrogen jet. Three of these positions are on the jet axis, while the remaining two positions are in different horizontal distances to the jet centerline (see **Fehler! Verweisquelle konnte nicht gefunden werden.Fehler! Verweisquelle konnte nicht gefunden werden.**). Since these sensors are quite large and require a constant gas flow they were not mounted physically to the

positions shown in **Fehler! Verweisquelle konnte nicht gefunden werden.**, but were connected to these positions via thin plastic tubes of 2.55 m length. One small pump is used to supply all sensors with the same volume flow of test atmosphere during the measurements. In pre-tests the delay time with this setup was determined by exposing the open tip of the plastic tube with pure or diluted hydrogen (20% H_2, forming gas) from a balloon (without forcing an additional flow of the test gas in the tube). A delay time of 2 s was found for all five sensors in this setup from the opening of the hydrogen balloon to the first increase in the signals of the hydrogen sensors. After further pre-test plastic tubes with tilted cut ends were used.

Field mills: Two electric fieldmills (model Kleinwächter EFM 113B) were positioned in the height of the nozzle in distances of 0.5 and 1.5 m from it and with horizontal distances of 0.9 m from the jet axis (see **Fehler! Verweisquelle konnte nicht gefunden werden.**). The electrostatic field strength determined with the fieldmills was exploited in work package WP4 Ignition. No further reference is made in this report.

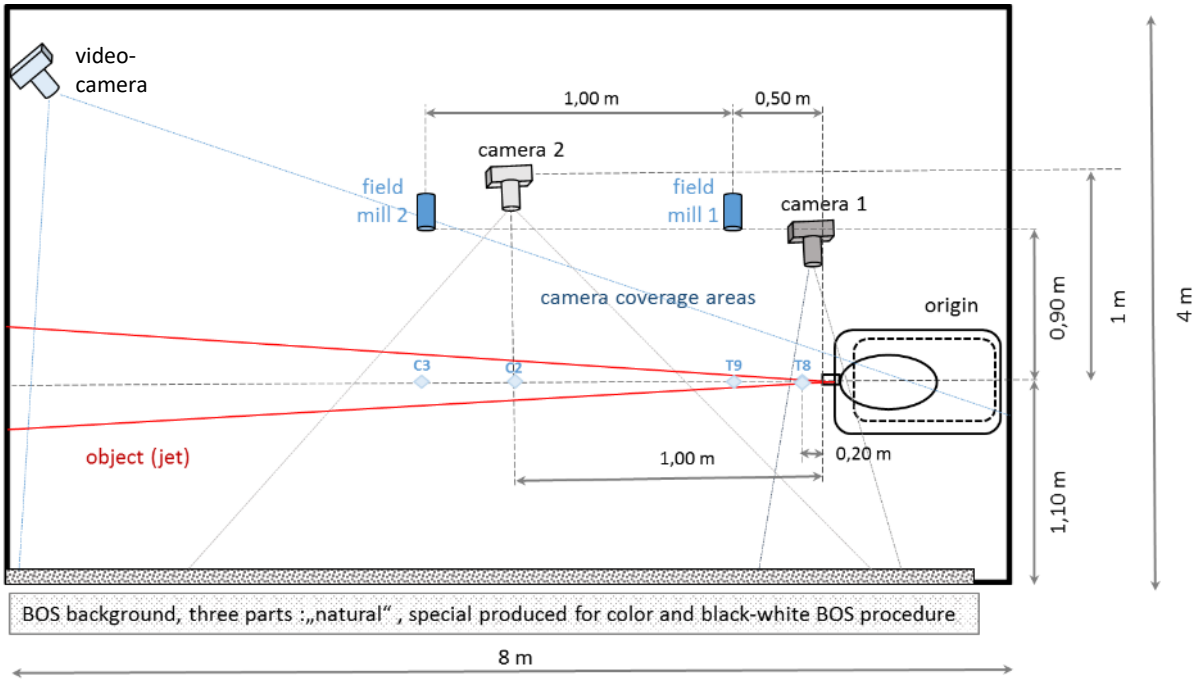

Figure 5: Sketch of the positions of the electric fieldmills and the cameras in the DISCHA-facility (top view).

Cameras: The two photo-cameras were positioned at 5 cm (Camera 1) and 1 m (Camera 2) in jet downstream direction, on the same height as the center of the release nozzle and with a distance of 0.9 m (Camera 1) and 1.1 m (Camera 2) to the horizontal center line, the nominal jet center line (see **Fehler! Verweisquelle konnte nicht gefunden werden.** and **Fehler! Verweisquelle konnte nicht gefunden werden.**).

The photos were synchronized with the release time by utilizing the high-speed optical clock (see **Fehler! Verweisquelle konnte nicht gefunden werden.** left) also used for determination of the opening times of the ball valve.

The video-camera was positioned below the roof of the tent in a distance of several meters downstream the nozzle pointing towards the release. To the streamwise left of the released gas jet, opposite to the two photo-cameras, different background patterns were mounted on wooden walls. In the domain close to the nozzle a fine random black and white box-pattern was used, while in farther distances similar stochastic patterns and "natural" backgrounds (branches and shrubs) were applied.

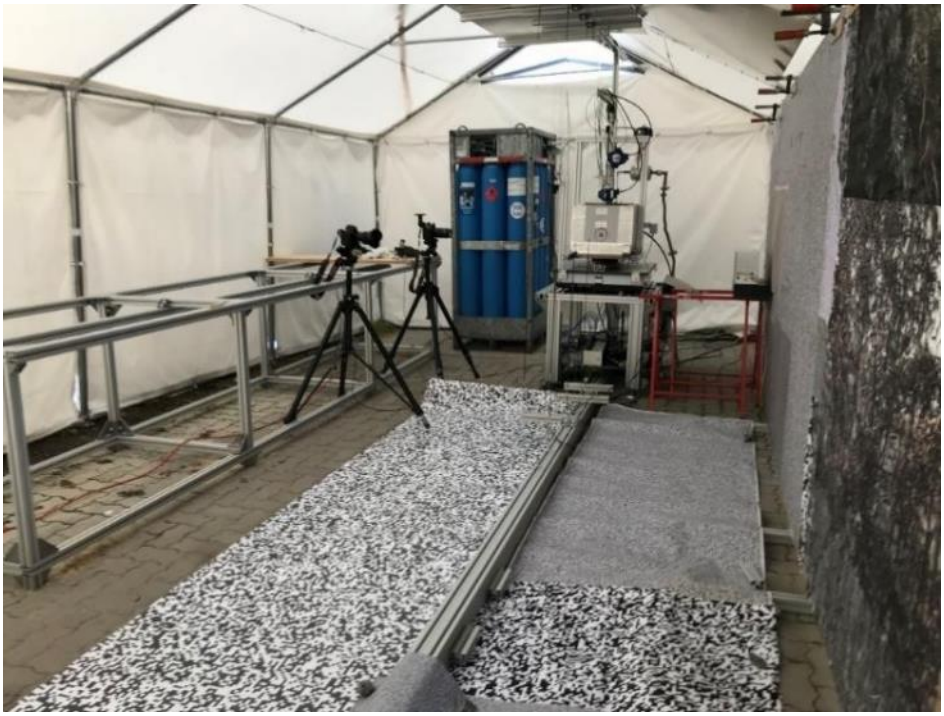

Figure 6: Position of cameras and BOS background patterns on floor and back wall.

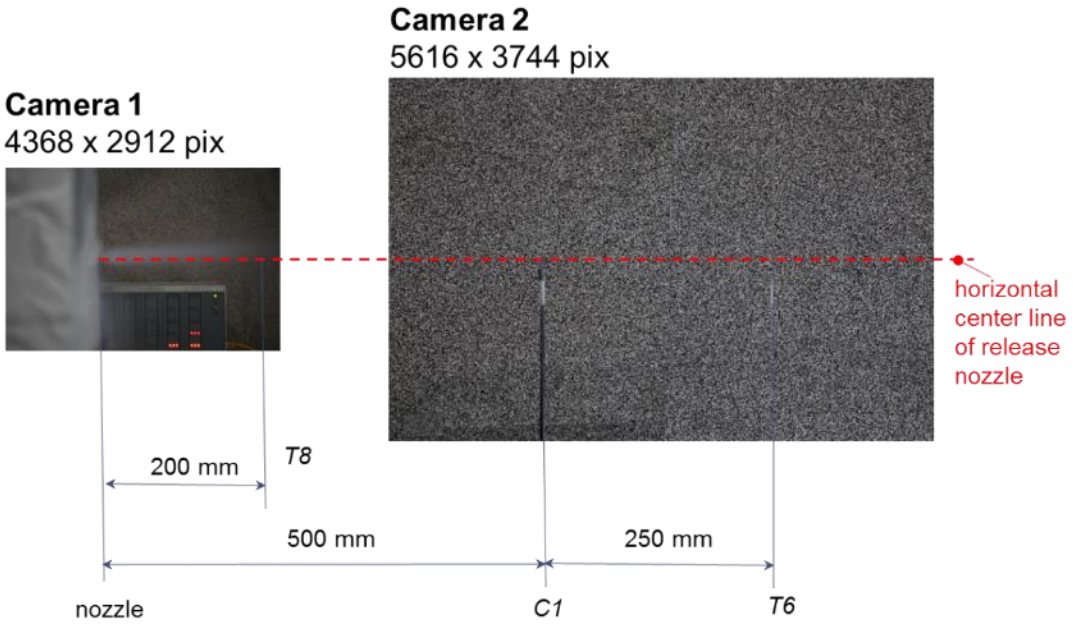

Figure 7: View fields of the cameras and BOS backgrounds applied (nozzle on the left end of the horizontal center line; thermocouples T8 and T6, concentration sensor C1), optical clock on visible for Camera 1.

2.2.1 Estimate of Measurement Errors

The accuracy of the sensors used in the experiments is given in Table 3. The values were taken from the respective manuals for ambient temperature conditions. For cryogenic temperatures no data is available.

Table 3: Accuracy of the sensors used in the DISCHA experiments.

Sensor	Manufacturer	Type (Range)	Non-linearity @ 290 K
Force	Althen	ALF318CPR0K0 (2 kN)	± 0,1 % FS
Scales	Mettler-Toledo	PBA430x (150 kg)	0.006% FS
Pressure	WIKA	S-20 (250 bar)	< 0,125% FS
Field mill	Kleinwächter	EFM 1138 (5 kV/m)	< 5% FS
H_2-Sensor	Messkonzept	FTC300 (100% H_2)	< 1% FS
Temperature	KIT-Workshop	Type K, d = 0.36 mm	1.66 °C

In the experiments only the thermocouples are exposed to cryogenic temperatures and so their deviation from the temperature of LN_2 (77 K) was measured in a separate low temperature calibration test. In this test all closed thermocouples showed similar values of approx. 84 K, what corresponds to a difference of +7 K. The three open thermocouples T1o, T2o and T3o, used additionally inside the test vessel, were also tested in the same way, but showed quite large deviations with values of approximately 105 K for the temperature of liquid nitrogen. The reason for this behavior might be rooted in the unprotected open sensor tip, which might be degenerated by the special application and by their application history. However, because of their lower thermal capacities, their

signal was used to determine characteristic changes in time rather than to read accurate, absolute temperature values.

2.3 Test matrix of the DISCHA experiments

The test matrix for the blow-down experiments was constructed by varying the release nozzle diameter (4 diameters: 0.5, 1, 2 and 4 mm) and the initial hydrogen storage pressure (7 nominal pressure values: 0.5, 1, 2, 5, 10, 15 and 20 MPa) for two hydrogen storage temperature levels (2 nominal storage temperatures: 80 and 300 K). Typically, at least three repetitions of one pressure/nozzle diameter combination were conducted. In many cases the test has been repeated more than three times, for 20 MPa and 2 mm even seven tests were done to provide an estimate for the stability, reproducibility respectively, of the measurement system in general.

The whole test campaign with more than 224 tests lasted almost 4 months (middle of February to end of June 2019) with several interruptions for improving the measurement set-up, setting up the pre-cooling or because of delays in LN_2 supply. Several pre-tests have been excluded from this report.

The test itself and the respective result files are labeled with the date and time ("date"_"time"), at which the test was initiated:

2019**MMDD_hhmmss**(.**ext**)

with **MM** for month, **DD** for day, **hh** for hour, **mm** for minute, **ss** for second of the formal start of the experiment; **ext** is either empty for just labelling the experiment, "xlsx" for the Excel files containing the dataset or "zip" for the set of photographs, pictures respectively, taken from this experiment.

The labeling convention of the zip-files containing several of those data or picture files for identical nozzle diameter and temperature follows this scheme:

PRE3P1A_KIT_D**X_YY**K_(**PICS**/**DATA**).zip

with X for nozzle diameter / mm and YY reservoir temperature / K. The test matrix for the cold experiments done with LN_2 cooling - the actual cryo-release tests - is shown Table 4. The datasets published on KITOpen [1] are highlighted with black bold font. The labels of those experiments, for which photographs are published have a grey background color. The cold test 20190528_104204 (i.e. the test, which started 28th of May 2019 at 10:42 am) and for photography 20190503_140045 are used as reference in the detailed description provided as metadata on KITOpen.

Table 4: Test matrix of DISCHA experiments at LN_2-temperature (n_{total}= 98, experiment label 2019MMDD_hhmmss for start date and time)

		Nozzle-Diameter [mm]			
		0.5	1	2	4
Pressure	5	20190509_143959 20190509_144955 20190604_151150 **20190604_153521**	20190507_155308 20190507_160047 **20190531_120333**	20190430_150817 20190430_151117 **20190531_103828**	20190503_112024 20190503_112408 **20190528_111918**
	10	20190509_142254 20190509_143252 20190604_150515	20190507_153753 20190507_154609 20190531_115603	20190430_144909 20190430_150600 **20190531_103408**	20190503_110955 20190503_111525 **20190528_111240**

		20190604_152905			
	20	20190509_111408 20190509_112201 20190604_145638 **20190604_152254**	20190507_152321 20190507_153041 **20190531_114903**	20190430_143105 20190430_144308 **20190531_102810**	20190503_110259 20190503_121635 **20190528_110441**
	50	20190509_135757 20190509_141151 20190604_144425	20190507_150252 20190507_151256 20190531_113940	20190430_141445 20190430_142516 **20190531_101948**	20190503_115334 20190503_120719 **20190528_105437**
	100	20190509_132731 20190509_134535 **20190604_142752**	20190507_143257 20190507_144631 **20190531_112944**	20190423_120305 20190430_111836 20190430_114028 **20190531_101249**	20190503_104121 20190503_105250 20190528_112837 **20190528_143608**
	150	20190509_104138 20190509_105344 20190604_140657	20190507_135605 20190507_141457 20190531_111808	20190423_121441 20190430_135153 20190430_140732 **20190531_100257**	20190503_100144 20190503_102600 **20190528_142048**
	200	20190509_100955 20190509_102557 **20190604_134543**	**20190531_110440**	20190430_102456 20190430_110643 **20190531_094951**	20190503_134536 20190503_140045 **20190528_104204**

Published Excel **datasets** for instance in:
PRE3P1A_KIT_**D1_80K**_DATA.zip
corresponding photographs in
PRE3P1A_KIT_**D1_80K**_PICS.zip

Legend:
Not processed, sync. difficult
Processed, wrong format, sync. difficult
~~Processed, no sync.~~
Processed and synchronized
Published Photographs
Published Datasets
used for further explanations

2.4 S E3.1a

In the frame of the E3.1a test series of the PRESLHY own experiments were made and evaluated using the DISCHA-facility of KIT. 98 of the experiments were made at cryogenic temperatures, close to the standard boiling temperature of nitrogen (approximately 80 K) and 126 at ambient temperature (approximately 300 K). The measurement of pressure, temperature and concentrations in the pressure vessel and in the released jet was steadily improved. Only the most mature and reliable dataset have been published on KITopen.

The inventories stored in the DISCHA pressure vessel for those blow-down experiments vary from about 1.2 g, for the lowest pressure 0.5 MPa and ambient temperature, to about 140 g, for the highest pressure 20 MPa and standard boiling temperature of nitrogen. Table 5 contains the densities for the relevant conditions and the corresponding inventories in the DISCHA vessel with 2.815 dm^3 free volume. The densities have been derived with real gas factors extracted from [2].

Table 5: Hydrogen inventories of the DISCHA experiments.

Temperature / K	Pressure / bar	1	5	10	20	50	100	150	200
293,15	Ideal Density / (g/l)	0,083	0,414	0,827	1,654	4,136	8,271	12,407	16,542
	Z -factor @ 300 K	1,000	1,000	1,008	1,013	1,030	1,060	1,090	1,120
	Density / (g/l)	0,083	**0,414**	**0,821**	**1,633**	**4,015**	**7,803**	**11,382**	**14,770**
	H2 mass in DisCha / g	0,233	**1,164**	**2,310**	**4,597**	**11,303**	**21,966**	**32,042**	**41,578**
77	Ideal Density / (g/l)	0,315	1,574	3,149	6,298	15,745	31,490	47,235	62,980
	Z -factor @ 80K	1,000	0,990	0,980	0,970	0,960	1,020	1,130	1,260
	Density / (g/l)	0,315	**1,590**	**3,213**	**6,493**	**16,401**	**30,872**	**41,801**	**49,984**
	H2 mass in DisCha / g	0,886	**4,477**	**9,045**	**18,277**	**46,169**	**86,906**	**117,669**	**140,704**

Even for the experiments with highest inventory the weight and the repulsive force measurements show considerable noise, perturbations and limited precisions, see Figure 8. So, these data should be considered rather qualitative than quantitative. Best quality is provided in the pressure recordings.

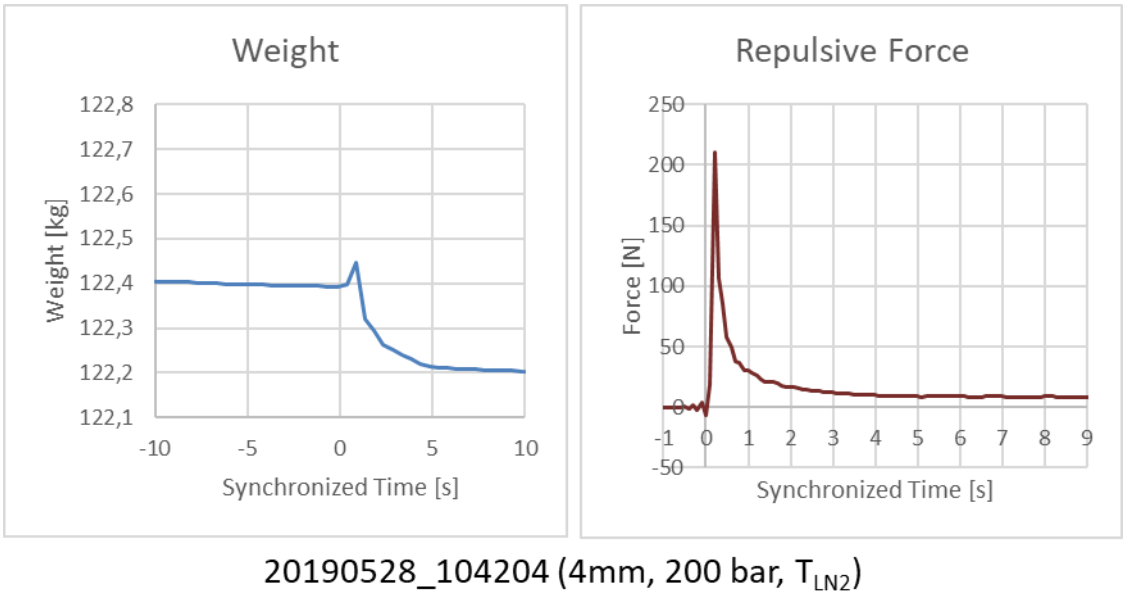

Figure 8: Weight and repulsive force measurements of the DISCHA set-up for hydrogen blow-down starting with 200 and nitrogen boiling temperature

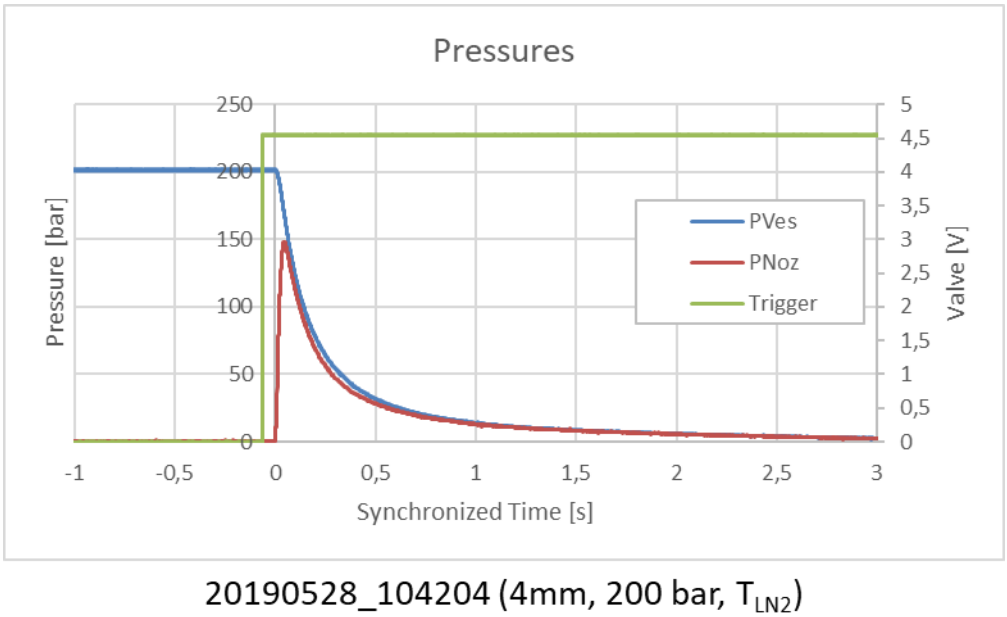

Figure 9: Pressure measurements in the vessel and release line before the nozzle and trigger signal for hydrogen blow-down starting with 200 bar and nitrogen boiling temperature

As explained above all experiments with identical temperature, pressure and nozzle diameter combination have been repeated at least three times (with the only exception of the cold test with 10 MPa and 1 mm nozzle diameter). The test series with 4 mm nozzle at ambient temperature with a pressure of 10 MPa provide 8 and the 20 MPa 7 repetitions and allow for a statistical evaluation of the measured reservoir pressure. The root-mean-square deviation (RMSD) for the two test series was calculated and for 10 MPa it is less than +/- 0.5%. For 20 MPa it is about +/- 1%.

Some general results of this experimental campaign are:

- Not a single test showed a spontaneous ignition
- The tests done with hydrogen at ambient temperature do not generated any significant electrostatic field, whereas the cold jets generate relative strong static electricity, in the order of 5 kV/m. This is 100 - 1000 times stronger than the natural electrostatic background field. The strong static electricity seems to be generated by ice crystals (potentially water ice from ambient humidity) which form on the release nozzle before the tests. The jet entrained electric charge is in some cases positive in other cases negative. These findings are supported by similar pre-cursor experiments done at KIT, and are further exploited in work package WP4.
- In all cold tests white fog was generated in the jet domain. It is assumed that this is mainly attributed to the ambient humidity, which condensates in the cold entrainment zone. The weather conditions for late April to early June at the experimental site (KIT Campus North) had a minimum relative humidity of 35% at 32°C, experiments in the afternoon of 4 June 2019, and a maximum humidity of almost 100% in the morning of 9 May 2019. Qualitatively the visible cloud seem to coincide with flammable gas compositions. Also this finding should be further refined and checked against dependency on humidity levels.
- The cold tests with large diameter and high pressure show strong temperature decay in the reservoir and a quite strong fog generation. However, as stated above it is currently assumed, that these particles are water droplets and ice crystals from ambient humidity. The latter originate at least partially from ice crystals formed on the nozzle before the actual test. It may not be excluded that there is involved condensation of other gases, like CO2, oxygen or even hydrogen, as the acceleration during the release might bring down the dynamic temperature even below the hydrogen boiling point. Only detailed multi-phase simulations accounting for non-equilibrium effects might clarify this issue.
- The fog generated impaired the BOS methodology, in particular in the far field measurements.

3 Experiments E3.1b – Discharge from CRYOSTAT facility

3.1 General Description of the CRYOSTAT-Facility

To complement the DISCHA tests and to cover LH2 temperatures in the order of 20 K discharges from a LH2 cryostat were included in the experimental program for release and mixing of PRESLHY project. Pre-calculations on the expected hydrogen mass flow for the maximum release conditions were performed and proved that the released amount of H_2 is too large to be handled on KIT-HyKA in case of an unintended spontaneous ignition (P_{ini} = 0.5 MPa, d_{Noz} = 4 mm → $\dot{m}_{LH2}$ = 96.4 g/s), since there are several buildings with windows located in the vicinity. For this reason, the free-field test site of the Institute for Technology and Management in Construction (TMB), which is part of KIT Campus South, was loaned for the tests. This free field test site is located approx. 3.5 km north of KIT Campus North at the edge of the northern part of the Hardtwald forest (see Figure 10).

Figure 10: Location (left) and aerial view from the north (right) of the free-field test site north of KIT Campus North with later positions of the LH2-trailer (blue) experimental area (red circle) and tent for data acquisition (yellow).

The biggest cost factor in the procurement of LH2 for the experiments turned out to be the rental of the super-insulated trailer needed to store the LH2 for the duration of all experiments with LH2 at the test site. To keep these costs as low as possible it was decided to perform all experiments with LH2 within a time frame that had to be held as short as possible. So the facilities for all experiments with LH2 done by KIT/PS were prepared and stored at the free field test site north of KIT-Campus North before the LH2-campaign began with the delivery of the LH2-trailer.

The tests with the CRYOSTAT-facility were performed on the standard location for the LH2-tests on the free-field test site with the LH2-trailer parked close to it besides a massive steel container and with its rear end pointing towards the experimental area. Behind the rear door of the trailer, the control panel with all valves and joint points is located and thus this door had to remain opened during the withdrawal of LH2 from the trailer. For protection of this vulnerable part of the trailer a protective wall of concrete bricks (M = 500 kg/brick) was constructed between trailer and experiment. This rather crowded layout of the components was necessary due to the fact that the CRYOSTAT-

facility had to be filled with LH2 from the trailer through the rather short (L ≈ 5 m) super insulated hose that was provided by Air-Liquide together with the trailer (see Figure 11).

Figure 11: Photograph of the general set-up of the CRYOSTAT-facility.

The CRYOSTAT facility consists mainly of a LN_2-shielded stainless-steel cryostat with an internal volume of 225 dm^3 that was loaned for the tests from another institute at KIT. The main problem with this vessel was the missing lid with all connections, which had to be constructed and fabricated according to the needs of the experiment. The cryostat is designed for a maximum pressure of 0.6 MPa (absolute pressure, corresponding to 0.5 MPa overpressure). If the maximum pressure of the vessel is exceeded, an integrated safety valve opens automatically and depressurizes the facility. As further safety measure, several burst-discs are also installed. Figure 12**Fehler! Verweisquelle konnte nicht gefunden werden.** shows photographs of the CRYOSTAT vessel and a drawing of the special lid that was fabricated for the experiments.

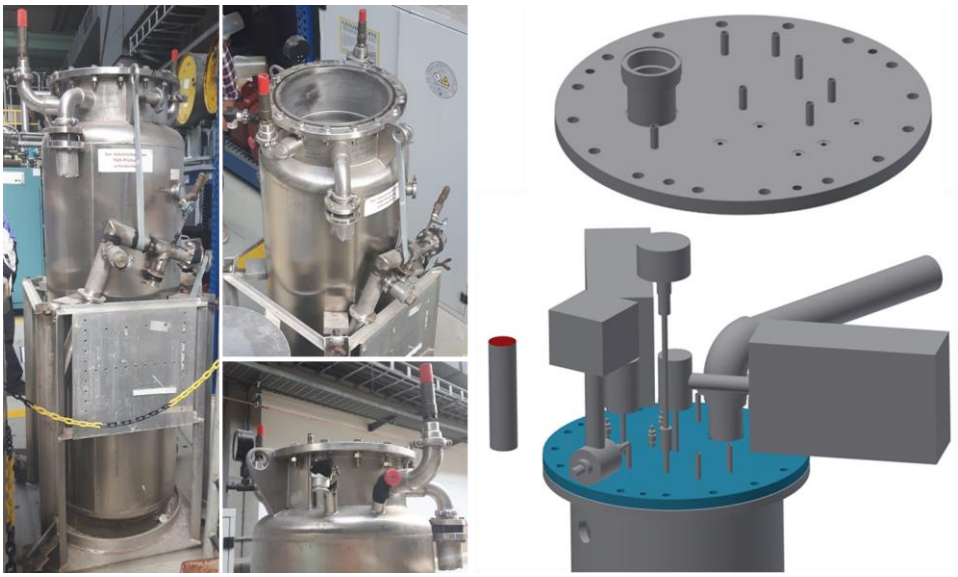

Figure 12: Photos of the CRYOSTAT-facility and technical drawing of the lid fabricated to house the components needed to realize a connection to the LH2-trailer as well as a LH2-release through the same release branch as used in the DISCHA-facility.

In the special lid of the CRYOSTAT, all components needed to realize a connection to the LH2-trailer as well as a LH2-release through the same release branch as used in the DISCHA-facility (see Figure 3 and Figure 13) are integrated. For the control of the filling level, a set of 5 thermocouples at different heights inside the vessel as well as a scale that measures the mass of the complete assembly are used.

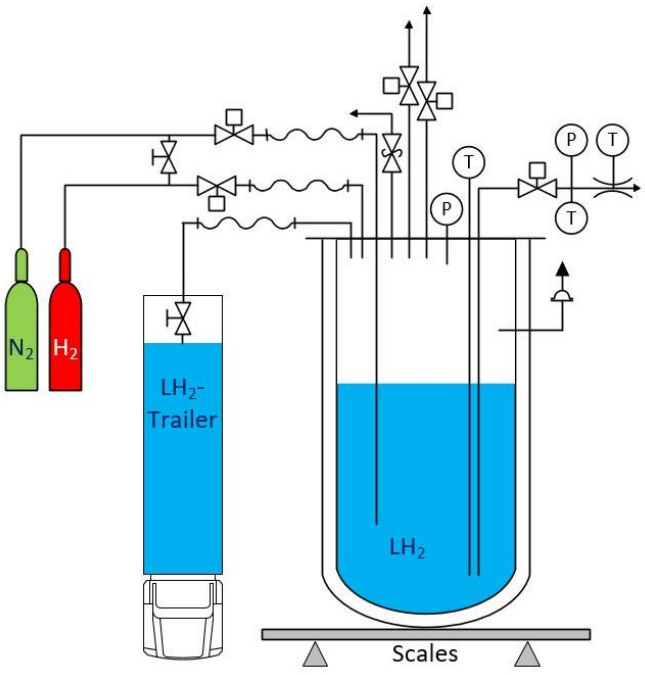

Figure 13: Sketch of the CRYOSTAT-facility with gas and LH2-supply and instrumentation.

While in the DISCHA-experiments four circular nozzle diameters were applied (0.5, 1, 2 and 4 mm), in the CRYOSTAT experiments only two of these nozzles (orifice diameter 2

and 4 mm) were used. These nozzles were the same as in the DISCHA-experiments and they were also mounted to the same tubes and joints connecting them with the same release valve (**Fehler! Verweisquelle konnte nicht gefunden werden.**). All tubes and the valve in the release branch have an inner diameter of 9 mm, while in the connectors the diameter is 9.5 mm. The complete release branch has a length of 367.4 mm from the end of the CRYOSTAT riser duct (or the end of the release tube welded to the DISCHA vessel) to the end of the nozzle orifice.

3.2 Sensors and Methods used in the CRYOSTAT-Facility

The complete CRYOSTAT-facility was mounted on a scale (Mettler-Toledo, Type: PFK989, range: 0 - 600 kg, Figure 14) to monitor the filling level of the vessel during the filling procedure and the release experiment. Special care was taken to eliminate influences of wires and hoses. The filling level of the vessel was also monitored using 5 thermocouples that were installed inside the vessel in different heights. Similar to the DISCHA-facility one pressure sensor was used to record the pressure inside the vessel throughout the complete experiment. Since the same release branch as in the DISCHA-experiments is used, a second pressure sensor and a thermocouple are installed to the junction in the release line between release valve and nozzle. Both pressure sensors are the same as in the DISCHA experiments (WIKA, Type: S-20, Range: 0 - 250 bar(rel.)), and also the thermocouple was unchanged since it cannot be removed from this junction.

With the CRYOSTAT facility blowdown experiments with gaseous and liquid hydrogen were performed. During the whole experiments the super insulated hose from the LH2-trailer was connected to its port on the lid of the cryostat. After assembly, the cryostat vessel was purged for more than one hour with gaseous nitrogen. Thereafter the vessel was purged with gaseous hydrogen from bottles for another half an hour before the vessel was sealed and the facility was prepared for the beginning of the experimental series.

In the first series with gaseous hydrogen the cryostat vessel was filled with H_2 from gas bottles up to the desired pressure, with some pauses and refilling phases to achieve thermal equilibrium. After the end of this series the shield chamber of the cryostat vessel, which is insulated against the ambience and the LH2-vessel by vacuum chambers, was filled with LN_2 to the prescribed level, while the H_2-pressure in the vessel was kept at a slight overpressure to eliminate air ingress from outside through potential leaks. Then the filling with LH2 was initiated by purging the cryostat vessel with the gaseous boil-off hydrogen from the LH2-trailer through the super insulated hose. With increasing time the flowing inflowing hydrogen becomes colder and increasingly more LH2 is purged into the cryostat vessel. During the complete filling procedure, the pressure inside the vessel is thoroughly monitored and kept at values in between 0.2 and 0.4 MPa(a) to exclude air ingress and to prevent the safety devices of the vessel from opening ($p_{max,CRYOSTAT}$ = 0.6 MPa(a)). When the desired filling level (i.e. weight of complete vessel) is reached, the bypass valve and the LH2-valve at the trailer are closed. The desired pressure in the vessel is then adjusted by cautiously adding gaseous H_2 from a bottle or by depressurizing through the bypass valve.

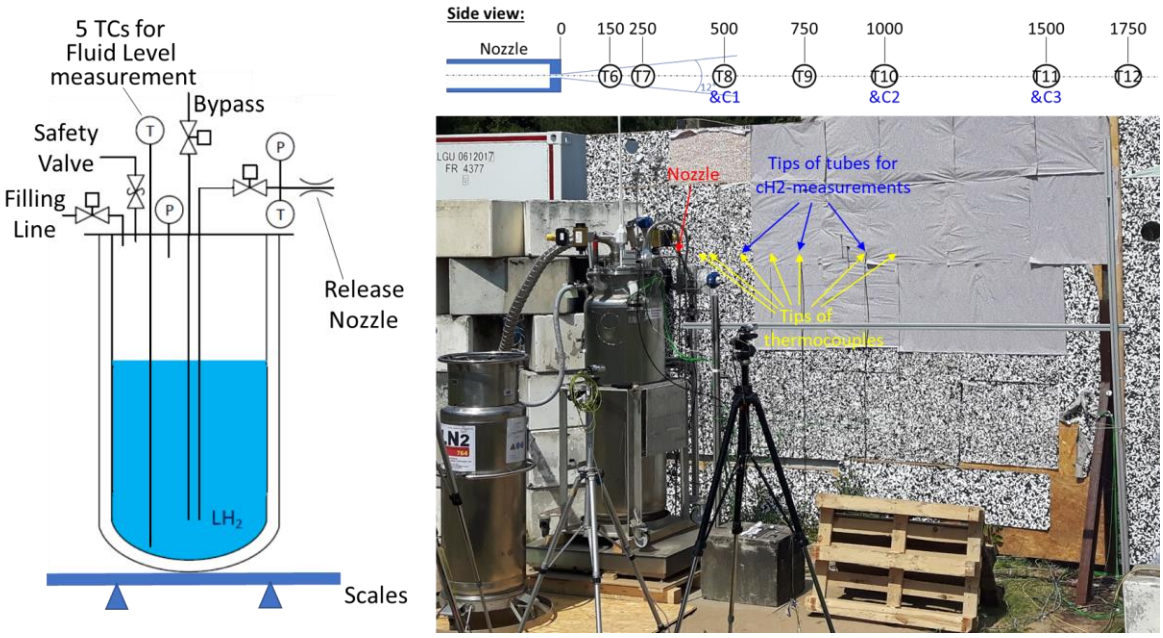

Figure 14: Sketch and photo of the CRYOSTAT-facility with details of the instrumentation.

Outside the release nozzle seven thermocouples and a set of three tubes for sampling based H_2-concentration measurements are installed in positions on the centerline of the jet. The distances of the sensors to the release nozzle are given in Table 6**Fehler! Verweisquelle konnte nicht gefunden werden.**.

Table 6: Distances of the sensor positions on the jet axis to the release nozzle.

Sensor(s)	T6	T7	T8 and C1	T9	T10 and C2	T11 and C3	T12
Distance from nozzle [mm]	150	250	500	750	1000	1500	1750

The seven thermocouples (Type K, diam. 1 mm, manufactured by KIT-workshop from same batch as in all other LH2-experiments, compare section on Estimate of Measurement Errors) were positioned with their tips on the jet axis using thin metal tubes that were adjusted on a horizontal profile rail in a distance of 50 cm below the jet axis.

For the concentration measurements plastic tubes had to be used to avoid disturbances of the flow due to the bulky H_2-Sensors and to provide a constant gas flow from the sampling position to the sensor. The tubes had a length of 10 m and were conducted through a water bath to provide for a gas flow with almost ambient temperature since the H_2-sensors must not be operated with cold gas of temperatures less than -60°C. The tips of the tubes with a tilted cut were positioned on the jet axis and fastened to the metal tubes that already stabilized the thermocouples.

Three field mills (Kleinwächter EFM 1138, measuring principle influence generator) for measuring static electric field strength and five cameras (2 photo cameras (C1 and C2), 2

video cameras (P1 and P2) and 1 thermo camera (IR)) are distributed besides the cold jet to monitor the releases using the BOS-technique for the visualization of density gradients (see Figure 15).

Pre-calculations of the expected hydrogen mass flow for the maximum release conditions were performed (P_{ini} = 0.5 MPa, d_{Noz} = 4 mm → $\dot{m}_{LH2}$ = 96.4 g/s). It proved that the expected mass flow is too large to be measured in separate pre-tests where the effused LH2 is evaporated and the gaseous flow is then measured by a flow meter at almost ambient temperature. Therefore, a scales method was chosen for mass flow measurements in which the mass of the effusing hydrogen is determined by weighing the complete facility.

To enable weight measurements the complete CRYOSTAT-facility was placed on the scale. The total weight of the experimental set-up, as measured by the scale is about 515 kg.

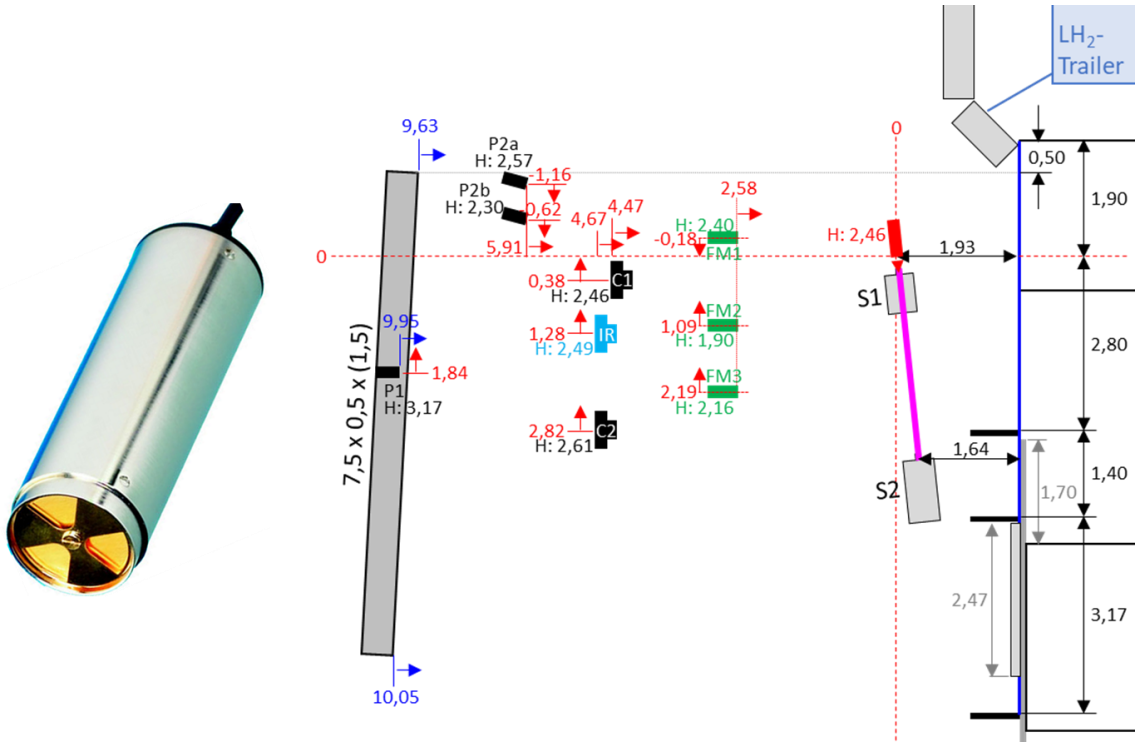

Figure 15: Field mill of type Kleinwächter EFM 113B (left) and sketch of the CRYOSTAT-facility with details of the instrumentation (right).

3.2.1 Estimate of Measurement Errors

The accuracy of the sensors used in the experiments is given in Table 7. The values were taken from the respective manuals for ambient temperature conditions. For cryogenic temperatures no data is available. All sensors were used in both series, unless stated otherwise.

Table 7: Accuracy of the pressure sensors, field mills and thermocouples used in the DISCHA- and the CRYOSTAT-experiments.

Sensor	Manufacturer	Type (Range)	Non-linearity @ 290 K
Pressure	WIKA	S-20 (250 bar)	< 0,125% FS
Field mill	Kleinwächter	EFM 1138 (5 kV/m)	< 5% FS
Temperature	KIT-Workshop	Type K, d = 0.36 mm	1.66 °C

In the experiments neither pressure sensors nor field mills were in direct contact with the cold hydrogen, so the accuracy for ambient temperature seems to be sufficient. However, the thermocouples were exposed to the cold gas and therefore these sensors were calibrated against LN_2 in a pre-test and against LH2 in the Pool-experiments that were conducted prior to the CRYOSTAT experiments. Using the three datapoints for ambient and the two cryogenic temperatures of LN_2 and LH2 a linear dependency was assumed with which all thermocouple records were corrected. The calibration curve for the thermocouples is shown in Figure 16.

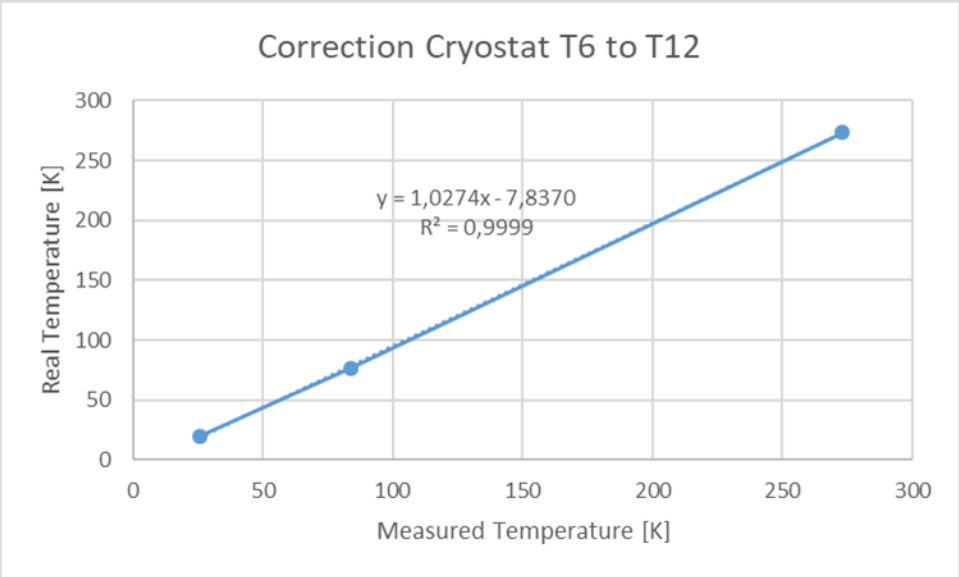

Figure 16: Calibration curve for the thermocouples used in the CRYOSTAT-experiments.

4 Experiments E3.4 – POOL evaporation tests

In the work package WP3 of the PRESLHY project the formation and evaporation behavior of liquid hydrogen (LH2) pools above different substrates are investigated within the experimental series E3.4 by the project partners Karlsruhe Institute of Technology (KIT) and Pro-Science (PS). In the work package WP4 the ignition and combustion behavior of cold clouds above these pools is analyzed.

4.1 General Description of the POOL-facility

For the experiments on LH2-spills the POOL-facility was built on the same free-field test site of KIT, which was also used for the CRYOSTAT tests (see Chapter 3).

Given the high costs of procurement and storage of LH2, it was decided to perform all LH2 experiments in a short time period. So all experiments had been prepared before calling for delivery of the pre-ordered LH2 in a trailer.

As for the other LH2 experiments the trailer was parked close to the experiments besides a massive steel container and with its rear end pointing towards the experimental area. Behind the rear door of the trailer, the control panel with all valves and joint points is located and thus this door has to remain opened during the withdrawal of LH2 from the trailer. For protection of this vulnerable part of the trailer a protective wall of concrete bricks was constructed between trailer and experiment.

This rather dense layout of the components was necessary due to the fact that the POOL-facility had to be filled with LH2 from the trailer through the rather short (L ≈ 5 m) super insulated hose that was provided by Air-Liquide together with the trailer. Opposite the wall with BOS background pattern another protective wall of concrete bricks was erected, in front of which usually all cameras for optical observation of the experiments were positioned, see Figure 17: Setup for the POOL-experiments with main parts of the facility (left) and sketch of the facility with dimensions (right)..

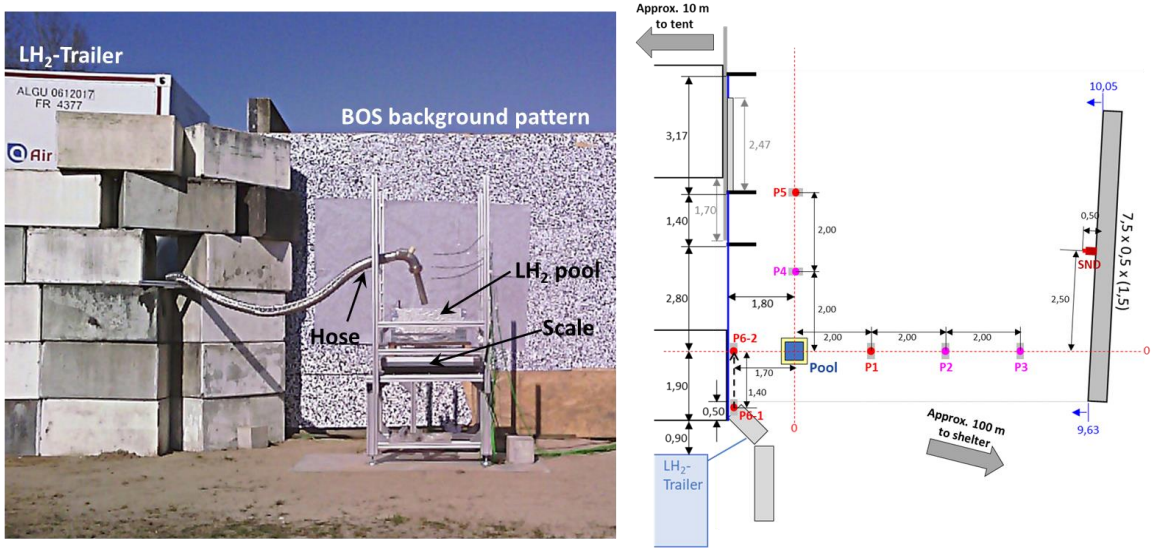

Figure 17: Setup for the POOL-experiments with main parts of the facility (left) and sketch of the facility with dimensions (right).

The POOL-facility was controlled via a control system that was located in a tent in a distance of approx. 10 m behind the wall with the BOS-background pattern. After the initiation of an experiment this control system was operated remotely via a master controler located in a shelter in a distance of approx. 100 m to the test facility (see Figure 18). The master controler was also used to display and save all sensor records (temperatures, H2-concentrations, ambient wind conditions) with a measuring frequency of 10 Hz via LabView.

The POOL-facility itself mainly consists of a stainless-steel box (dimensions 0.5 x 0.5 x 0.2 m^3) that is filled up to half the height (0.1 m) with different substrates that are relevant for various real LH2-applications. The substrates used in the tests were concrete, sand, water and gravel, with the concrete pool being prepared already more than 1 month prior to the first experiment to allow sufficient hardening and drying. Three boxes were fabricated for the experiments, so one of these boxes had to be used for the experiments with two substrates (water and gravel, gravel was kept in separate box when not used, so in all experiments with gravel the same stones were used as substrate). For thermal protection the outside of the boxes was insulated by Styrofoam plates on its bottom and side walls. Inside the substrate layer 8 thermocouples were positioned via holders prior to the filling of the box with the respective substrate. The substrate filled box was then positioned on a scale on a table and the super insulated hose from the LH2-trailer was then fixed to a rack on the top of the table that positioned its open end above the box. Photographs of the complete assembly and the empty as well as the substrate filled boxes are shown in Figure 18.

Figure 18: Photo of the setup of the POOL-experiments with LH2 on the free-field test site north of KIT-Campus North (top left) and photos of the empty stainless-steel box with in-substrate sensor holders (top right) as well as boxes filled with the different substrates (lower row).

For the LH2-release a hand valve at the rear end of the trailer had to be opened manually (always to the same degree of valve opening), but due to safety restrictions the closure of the release valve had to be done remotely using a safety mechanism of the trailer. In the experiments on LH2-pool formation the substrate filled box was usually filled three times to cover different degrees of pre-cooling of the substrate. Furthermore, it turned out that

all sensor records showed less fluctuations when the pool was generated above a per-cooled substrate. This data was needed to estimate the concentration in the ignition position for the ignited POOL-experiments of WP4.

4.2 Instrumentation of the facility

4.2.1 Sensors and Methods used

The insulated steel box of the POOL-facility was mounted on a scale (Mettler-Toledo, Type: PBA430x, 0 - 150 kg) to monitor the mass of LH2 accumulated in the pool during the filling and evaporation periods of an experiment. Special care was taken to eliminate influences of wires and hoses connected to the facility.

Thermocouples (TCs): 6 were installed about the substrate surface, to monitor the filling level of the pool. Further 8 thermocouples were distributed on holders inside the substrate. 12 thermocouples and 3 thin tubes for continuous sample extraction were positioned via wires in a rack above the box. Through the 3 thin tubes gas samples were transported from the sampling position to 3 H2-sensors that continuously analyzed the samples. All thermocouples used in the experiments were of the same type (sheathed thermocouples type K, d = 1.00 mm) manufactured at the KIT workshop from the same batch. The various thermocouple and sample taking positions used are sketched together with their names in the data records in Figure 19**Fehler! Verweisquelle konnte nicht gefunden werden.**.

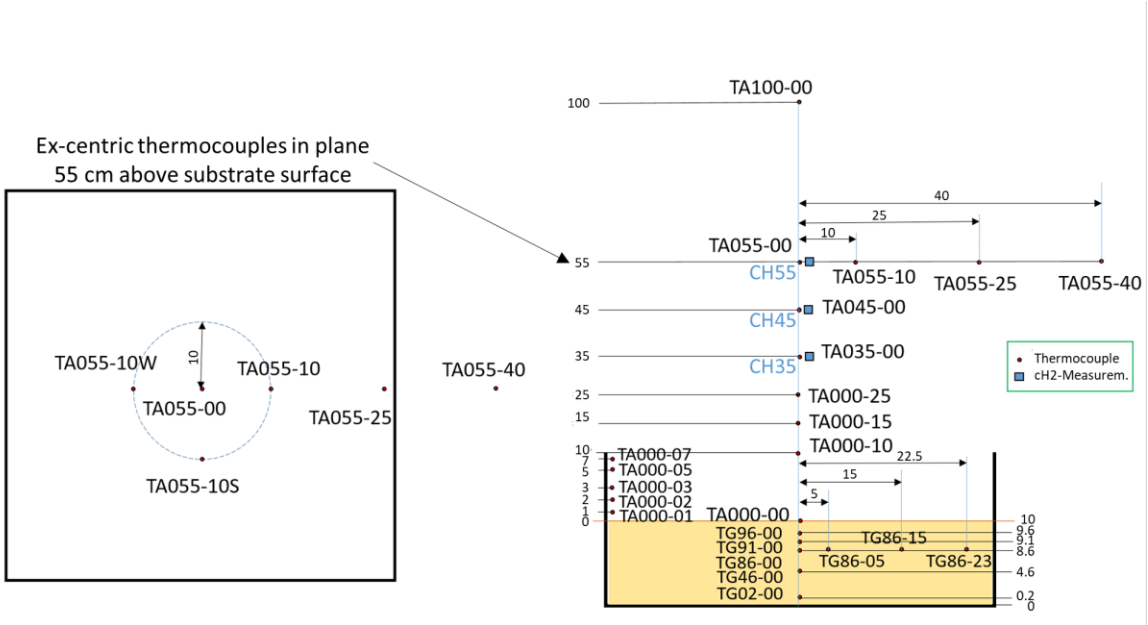

Figure 19: Names and positions of the thermocouples and cH2-measurement positions in and above the substrate (dimensions in cm)

Concentration measurements: 3 Messkonzept sensors (Model FTC300, 0 - 100 Vol% H2) were used. They had to be fed with a sample gas flow and always operated at temperatures higher than -20°C. For these reasons, they were installed behind the wall with the BOS-background, instead of above the pool. and to connect them with the sampling position via a thin cannula and a pump. This generates a time delay between the

time of extraction and of the actual measurement. This delay was determined in separate experiments as 35 s for all three H2 sensors.

In four experiments wind was generated with a large fan to investigate the influence of side wind on the LH2-pool formation and evaporation. To this end the fan was positioned in front of the wall of concrete blocks behind the trailer, to produce side wind of constant velocity and direction. In pre-experiments with an ultrasonic anemometer (Young, Model 81000) the rotation speed of the fan was tuned in a way that it produces wind with a velocity of approx. 4 m/s in the position of the center of the pool from the direction where the super insulated hose is fastened to the rack above the pool (Figure 20).

Figure 20: Photos of an experiment without artificial wind (left), the experimental setup with fan (center) and an experiment with artificial wind (right).

4.2.2 Estimate of Measurement Errors

The accuracy of the sensors used in the experiments is given in Table 8. The values were taken from the respective manuals for ambient temperature conditions. For cryogenic temperatures no data are available.

Table 8: Accuracy of scale, thermocouples, cH2-sensors and anemometer used in the unignited POOL-experiments.

Sensor	Manufacturer	Type (Range)	Non-linearity @ 290 K
Scale	Mettler-Toledo	PBA430x (0 - 150 kg)	< 0.006% FS
Temperature	KIT-Workshop	Type K, d = 1.00 mm	1.66 °C
H2-concentration	Messkonzept	FTC300 (0 - 100% H_2)	≤ 1% FS
Anemometer	Young	Model 8100 (0 – 40 m/s and -50 - +50 °C)	 ±0.05 m/s and ± 2 °C

Prior to the experiments the thermocouples were tested at ambient temperature in ice water and in a bath of LN2. All thermocouples showed very similar values for T_{ice} = 273 K (+/- 1 K) and T_{LN2} = 97 K (+/- 1 K), what corresponds to a precise measurement for 0°C and a deviation of approx. 20 K for LN2 temperature. As third point for the correction of all thermocouple signals the temperature measured by the thermocouples in the pool, which were exposed to LH2 in the experiments, was used. A LH2-temperature of 63.5 K (+/- 1 K) was measured by all these thermocouples, resulting in a deviation of

approx. 43.5 K at this temperature level. Unfortunately, the calibration curve for these three temperature levels is not linear, which offers three options for correction (Figure 21):

I. polynomial fit through the three temperature levels (red dotted line)
II. linear fit through the three temperature levels (orange dotted line) or
III. linear fit through values of LH2 and ambient temperature (black dotted line)

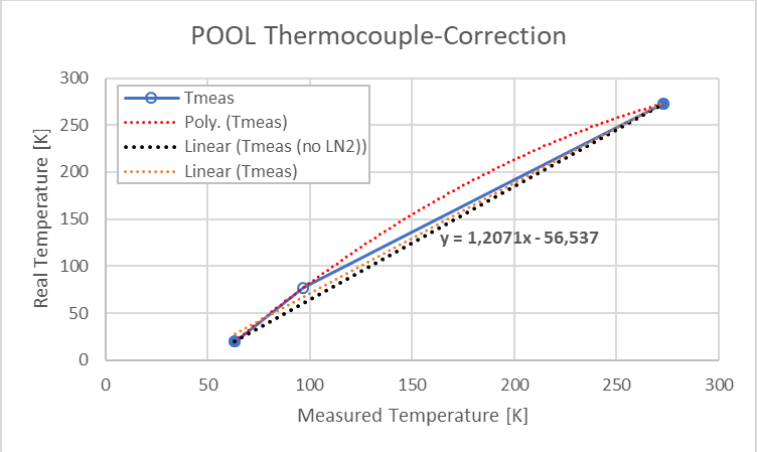

Figure 21: Calibration curve for the thermocouples used in the POOL-experiments.

Although option I leads to a perfect fit it seems to be worst since it produces a local maximum at approx. 300 K and all temperatures higher than this level do not lead to an increase of the corrected temperature. Option II shows the lowest deviations between measured and corrected temperatures for the three temperature levels, but for the boiling temperature of LH2 a value of 28 K is found. Finally, the third option displays an accurate value for the two extremal values (T_{LH2} and 273 K) but produces a deviation of -17 K for the boiling temperature of LN2 ($T(corr.)_{LN2}$ = 60 K). Nevertheless, this option was chosen since it facilitates interpreting the temperature records and so during data processing all temperature values were corrected using the black calibration line shown in **Fehler! Verweisquelle konnte nicht gefunden werden.** Figure 21.

4.3 Test Matrix and Experimental Data

4.3.1 Test Matrix and Data Structure

Table 9 shows the test-matrix for the 10 experiments of unignited LH2-spills that were performed with the POOL-facility and all four substrates available.

Table 9: Test matrix for the unignited POOL-experiments

Date	Substrate	Procedure	Conditions	Comments
20.03.2020	Concrete01	2 Fillings	Natural	No scales data (Not used)
24.03.2020	Concrete02	4 Fillings	Natural	
08.04.2020	Gravel01	3 Fillings	Natural	
09.04.2020	Sand01	3 Fillings	Natural	
15.04.2020	Sand02	3 Fillings	Wind	No natural wind data
16.04.2020	Sand03	3 Fillings	Wind	
17.04.2020	Concrete03	3 Fillings	Wind	
22.04.2020	Gravel02	3 Fillings	Natural	Gas-Samples
23.04.2020	Gravel03	3 Fillings	Wind	Gas-Samples
23.04.2020	Water01	3 Fillings	Natural	

Apart from the substrate mainly the wind conditions were varied in the tests. So apart from starting date and time the experiments the names of the 10 Excel-files with the sensor records of the unignited POOL-experiments also contain information on these variables. All filenames have the form:

2020**MMDD_substrateXX*Wind***

with **MM** for month, **DD** for day of the start of the experiment. **Substrate** indicates the nature of the substrate (either concrete, sand, water or gravel) and **XX** represents the total number of tests so far performed with the respective substrate. If an experiment was carried out with artificial wind the extension "***Wind***" is added to the name.

The string "TE-WG" is appended to the filename of the first sheet in the Excel file (e.g. "2020MMDD_substrateXX-TE-WG"). This sheet contains the data of all thermocouples and the weight record (see Figure 22**Fehler! Verweisquelle konnte nicht gefunden werden.**). All temperatures in this sheet are corrected values according to the black calibration curve given in Figure 21 (using the formula given in cell H1) with the exception of the thermocouple in column Q (highlighted red). The thermocouple initially planned for this column was not working properly in the first experiments and so it was replaced by one of the in-vessel-thermocouples of the DISCHA-experiments (T1 – T3, see Deliverables D3.4 and 5.4) to calibrate them also for LH2-temperature. In the course of the experiments with the POOL-facility all three DISCHA-in-vessel-thermocouples were used in positions close to the substrate surface and the records are given in this column. The values of this column are already corrected with the calibration curve described in the DISCHA report (using the formula given in cell Q1). In the columns B to G the temperatures inside the LH2-pool are listed, the columns H to S (ex. column Q, see above) contain the temperatures above the pool and the columns T to AA give the temperatures measured inside the substrate. The last column AB of this block corresponds to a virtual thermocouple that was planned to be used as a trigger, but was not necessary.

In the right part of the first Excel-sheet the scales-data is listed. This data had to be saved in a separate file due to the output settings of the scales, but, since this signal is very important for the evaluation of the experiment, it is added to the first sheet with the temperature records. The time scale of the scales-record is synchronized using the time the respective files were generated (Line 2 and 3 in the records, this data is not visible in **Fehler! Verweisquelle konnte nicht gefunden werden.** due to size reasons, in the data files it is displayed correctly). In the column AE the total mass of the facility is given,

while column AF lists the LH2-mass, which is calculated by subtracting the initial mass of the facility from the total mass.

In the left column of diagrams all thermocouples of the facility are plotted over time, with a summarizing plot at the top and details of the different fillings below. The second column of graphs shows the same signals separated for thermocouples in the substrate, in the LH2-pool and above the LH2-pool. The lowest graph in the second column shows details of the DISCHA-thermocouple signal for LH2-temperature. The single graph in the third column shows the transients of selected in-pool-thermocouples together with the original weight-record (total mass of facility) while in the fourth column similarly a summarizing and three detailed plots for the different filling procedures are given together with the LH2 mass. The two graphs in the right column summarize total mass (top) and LH2 mass (bottom) for the experiment.

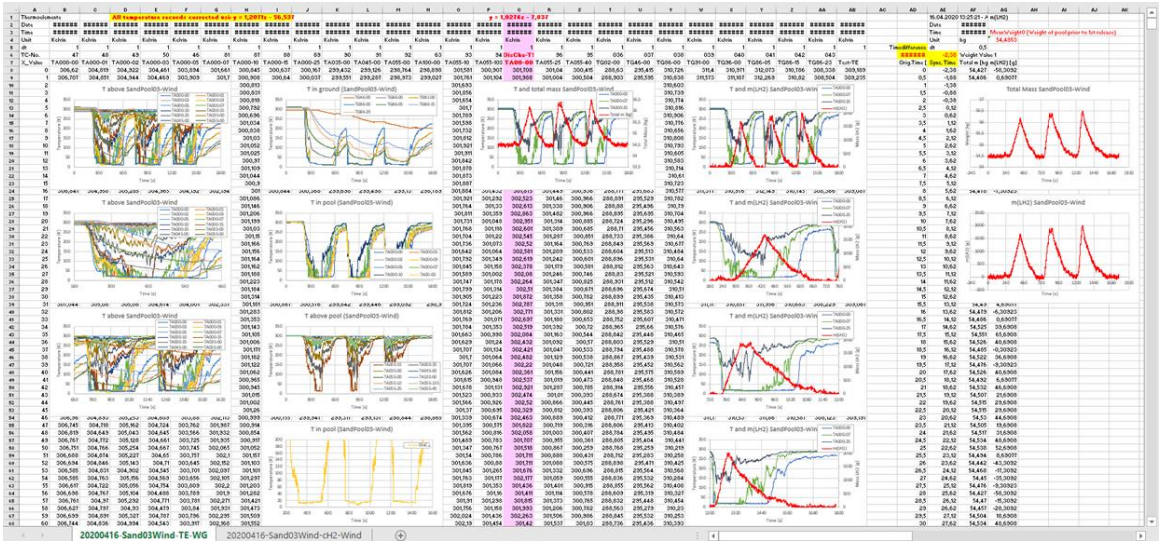

Figure 22: Example for structure of first datasheet on the basis of sheet "20200416-Sand03Wind-TE-WG".

In a second data sheet of the Excel-file the measured hydrogen concentrations and the wind data of the experiment are given and thus the extension "cH2-Wind" is appended to the sheet-name (e.g. "2020MMDD_substrateXX-cH2-Wind").

4.3.2 Explanations and Notes for Data-Interpretation

General behavior

The experimental data on the unignited POOL-experiments contains an enormous amount of individual sensor records, especially thermocouples. To facilitate the work with the data one example and several exceptional observations are explained next. For this purpose, Figure 23**Fehler! Verweisquelle konnte nicht gefunden werden.** shows the summarizing plot of the experiment 20200416-Sand03Wind as an example.

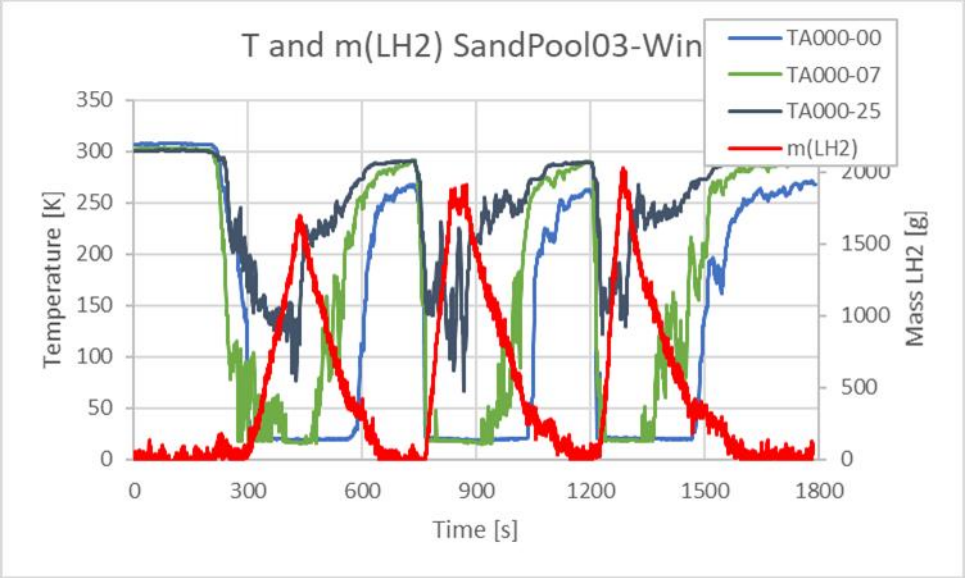

Figure 23: Summarizing plot of selected temperatures and the LH2-mass of experiment 20200416-Sand03Wind.

In the summarizing graph of Figure 23 the LH2-weight (red line, right ordinate) and the temperatures in three heights above the substrate surface are plotted. The slight weight increase and the fast temperature decreases at t ≈ 200 s indicate the LH2-release into the box. After an initial phase of cold GH2 as precooler, the LH2 starts then to reach the substrate surface and evaporates until the substrate surface is also cooled down to approximately 20K. As soon as a LH2-pool starts to form above the substrate surface (t ≈ 300 s) the signal of TA000-00 remains stable at the temperature of boiling LH2 (20 K) and the weight signal starts to increase. During the following 100 s the mass of LH2 in the pool increases constantly, as the increasing weight signal indicates, until the thermocouple in a height of 7 cm above the substrate surface is also reached by the LH2-level (t ≈ 400 s), as the stable value of 20 K measured by this sensor shows. Approx. 35 s later the LH2-release is stopped at a LH2-weight of approx. 1700 g, as the beginning decrease of the weight signal and the fast temperature increase in a height of 25 cm above the substrate surface indicate. The LH2-pool then evaporates constantly and reaches the filling level of 7 cm height at t ≈ 465 s, as the temperature increase measured by TA000-07 at this point in time shows. At t ≈ 580 s the temperature at the substrate surface starts to increase and thus the complete LH2-pool above the upper substrate level has evaporated. The remaining inventory of approx. 300 g at this time might be due to LH2 still existing in gaps between steel box and substrate as well as in between steel box and surrounding insulation material, or in pits that were formed by the fast flow of gaseous H_2 in the initial phase of the H_2-release. When the complete box had warmed to approx. ambient temperature in most measuring positions (t ≈ 740 s) the second filling was initiated. This time the pre-cooled substrate allowed a much faster filling of the box with LH2, as the quick temperature decay in both pool-thermocouples (TA000-00 and TA000-07) indicates. The pool was then filled to the upper rim (m_{LH2} ≈ 1900 g) and showed an overflow (t ≈ 835 s, stagnating weight) before the LH2-release was stopped (t ≈ 875 s). After this the LH2-pool evaporated to the same residual weight as after the first filling (m_{LH2} ≈ 300 g) until the temperature at the substrate surface starts to rise (t ≈ 1040 s). The third filling begins at t ≈ 1200 s and ends at t ≈ 1290 s and shows a course very similar to

the second one ($m_{LH2max} \approx 2000$ g). When the third LH2-pool had evaporated ($t \approx 1470$ s, $m_{LH2} \approx 350$ g) it was left to warm up to ambient temperature before the data acquisition was stopped.

Exceptional behavior

Gaps and ditches

A special phenomenon that occurred during in test described above, is connected with the residual weight that remains in the signal of the scale although the LH2 pool had completely evaporated (as shown by the signal of TA000-00 at the upper substrate surface). The explanations given above can be supported by the upper photos of Figure 24, where the gaps and the ditch in the sand are shown. Frozen humidity or air components are also feasible, but the temperature records show no hints on the evaporation of significant amounts of these compounds (no temperature stagnation at the respective boiling point).

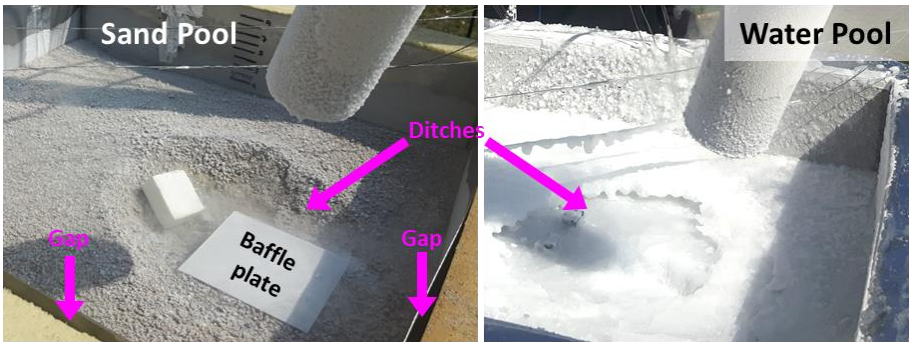

Figure 24: Gaps in between steel box and insulating material and ditches observed after experiments with the sand and the water pool.

However, gaps opened due to the thermal stresses in the metal walls of the box. The gaps were closed with tape prior to each experiment after they were realized for the first time (after experiment Concrete02). Unfortunately, they could not be closed reliably for various reasons (e.g. grounding of box, thermal stress in tape), and were unavoidable in the experiments with the substrate concrete, since stresses also occurred between the concrete and the metal of the box walls.

To avoid the phenomenon of ditches in the sand pool a baffle plate was used. This plate helped, but could not prevent the formation of a ditch especially during the first LH2-release, where a strong flow of gaseous H2 was directed into the bed of dry sand. Ditch formation was also observed in all experiments with the water pool, where no baffle plate could be installed. So in these experiments the effect is even stronger (also in first experiment with sand pool), which leads to an initial weight decrease of the pool due to the substrate that is blown out of the box before it is stabilized due to freezing.

Temperatures below 20 K and pool inventories of >> 2 kg

Another surprising phenomenon is the occurrence of temperatures below 20 K in some experiments when the pool is completely filled and is overflowing. The thermocouple connectors were identified as potential explanation for these obviously faulty measurements. The connectors were initially located unprotected on the outside of the pool insulation. When exposed to very cold temperatures the contacts in the connectors generate a second temperature sensitive element in the measuring chain and thus corrupted the temperature signal. In later tests this influence was avoided by shielding and insulating the connectors.

4.4 Preliminary Evaluation on the Basis of Experiment 20200423-Concrete02

A preliminary evaluation of potential results that can be gained from the data of the unignited pool experiments is briefly explained on the basis of experiment *20200423-Concrete02*. The summarizing plot with two temperatures and the mass of LH2 in the pool is shown in Figure 25.

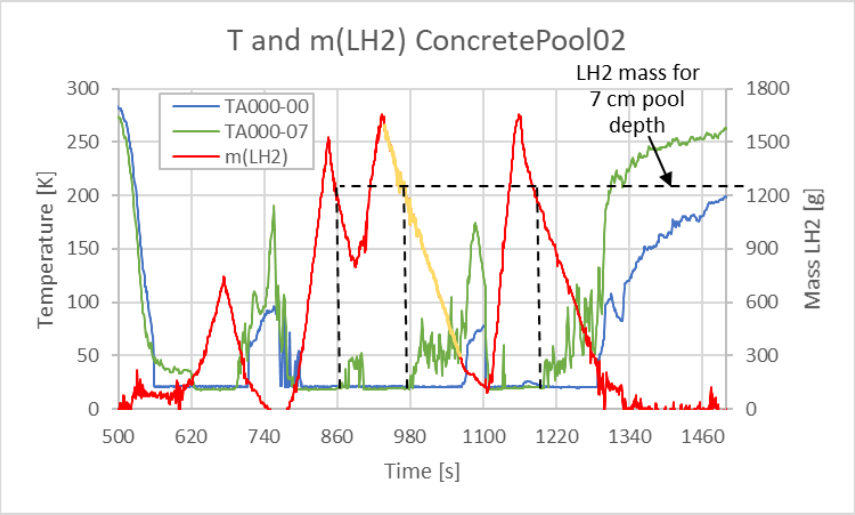

Figure 25: Summarizing plot of experiment 20200423-Concrete02 with two temperatures and the mass of LH2 in the pool. The yellow highlighted part of the weight curve is used for the determination of the weight-loss velocity.

As explained before the thermocouples (TC) records show a fast temperature increase from approx. 20 K to higher gas temperatures as soon as they are no longer covered by LH2. When these points in time are searched in the signal of TA000-007 (positioned 7 cm above substrate surface), the times when the LH2-level passes a height of 7 cm during the evaporation process can be determined (dashed vertical black lines in Figure 25). For the three points in time found in the signal of TA000-007 roughly the same LH2-mass in the pool of approx. 1240 g can be determined (horizontal black line). When the LH2-pool has completely evaporated (increase in signal of TA000-000 positioned at substrate surface) a remaining additional mass of approx. 300 g due to LH2 in gaps or other frozen compounds is still measured by the scale.

So, the actual mass of hydrogen in the pool at the point in time when the filling level decreases below 7 cm is approx.

$$M_{LH2pool@7cm} = 1240\ g - 300\ g = 940\ g \quad (1)$$

A pool of 7 cm height above a square base area of 50 cm side length has a volume of

$$V_{LH2pool@7cm} = 5\ dm \cdot 5\ dm \cdot 0.7\ dm = 17.5\ dm^3 \quad (2)$$

This results in a density for the LH2 in the pool of

$$\rho_{LH2pool} = 940\ g / 17.5\ l \approx 54\ g/l \quad (3)$$

which is low compared to a value of $\rho_{LH2} \approx 71$ g/l found in literature. This indicates that the pool contains an amount of approx. 76% LH2 and 24% void.

For the yellow highlighted part of the weight-curve in **Fehler! Verweisquelle konnte nicht gefunden werden.**, a weight loss velocity of

$$dm_{H2}/dt = 1301\ g / 124.5\ s \approx 10.5\ g/s \quad (4)$$

can be determined.

After the second filling ($t \approx 935$ s) the pool is completely filled to 10 cm height and LH2 begins to vaporize. When the LH2 level reaches a TC position the temperature jumps to a higher gas temperature, highlighted by magenta arrows in left part of Figure 26 for the pool-TCs from 10 to 0 cm height above the substrate surface.

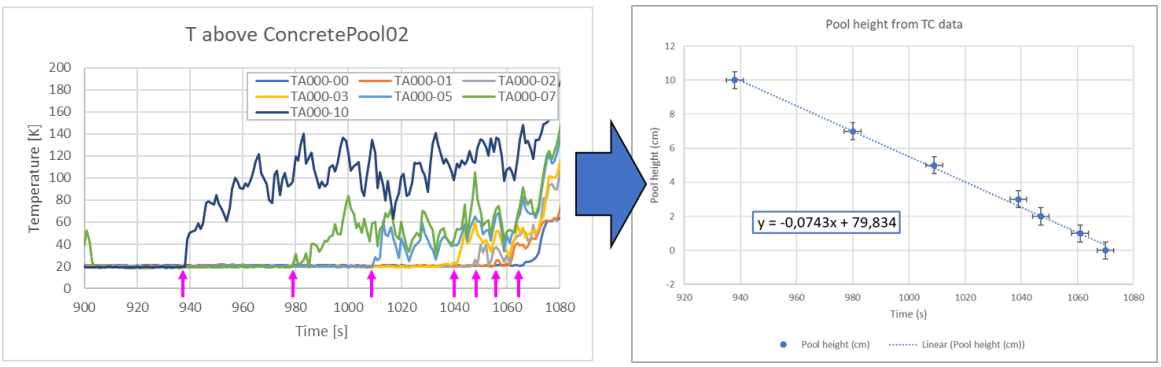

Figure 26: Determination of LH2-pool evaporation rate on the basis of TC-signals.

When these heights of the pool are plotted over time a vaporization velocity of the boiling LH2 pool in the form of a height reduction velocity $(dh/dt)_{boil}$ can be determined. With the relation

$$dm_{H2}/dt = \rho_{boil} \cdot L^2 \cdot (dh/dt)_{boil} \quad (5)$$

in which dm_{H2}/dt is the measured weight loss rate of the pool from Eq. (4), L is the side length of the square pool, $(dh/dt)_{boil}$ is the recession velocity of pool surface determined graphically in the right graph of **Fehler! Verweisquelle konnte nicht gefunden werden.**, and ρ_{boil} is the density of boiling pool.

When Eq. (5) is solved for the density of the boiling pool a value of $\rho_{boil} = 59.2$ kg/m³ is obtained, which corresponds to 83% of the LH2 density at 0.1 MPa pressure (71 kg/m³) and a GH2 void fraction of 17%, which is close to the estimated value of 24% void determined above.

The thermocouple data confirm the existence of a constantly evaporating two-phase LH2 pool which seems to be in the nucleate boiling regime.

The LH2 supply, the weight loss of the pool was measured with the high precision scale. A linear mass reduction rate, corresponding to a constant LH2 vaporization rate, was observed over extended time periods, from t_0 to t_{end}, as listed in Table 10.

Table 10: Characteristics of the four vaporization periods of experiment 20200423-Concrete02

Vaporization period	t_0 [s]	t_{end} [s]	m_0 [g]	m_{end} [g]	$\Delta m/\Delta t$ [g/s]	Heat flux q_{pool} [kW]
First	683	716	721.8	196,8	15,91	7,14
Second	856	893	1445.8	863,8	15,73	7,06
Third	949.5	1073.5	1560.8	253,8	10,95	4,73
Fourth	1180.5	1295.5	1367.8	265,8	9,58	4,30

The heat flux from the concrete into the LH2 pool was estimated as $q_{pool} = (\Delta m/\Delta t)\, \Delta h_{fg}$. The evaporation rate ($\Delta m/\Delta t$) and the corresponding heat flux from the concrete into the LH2 pool decreased with increasing time due to the decreasing temperature gradient in the concrete. The area of the concrete surface is A = 0.25 m² and the heat flux in W/m² is:

$$Q = q_{pool} / A = 4\, q_{pool} \quad (6)$$

The measured heat flux from the concrete Q is then in the range of 17.2 to 28.6 kW/m². Compared to these values, the heat flux to the pool from solar radiation is negligible, since, with the solar constant (1361 W/m²), a partial reflection of 25% on a clear day, and the solar inclination angle α for the time and location of the test (March, 49° northern latitude, α = 45°) Q_{solar} is approx. 0.72 kW/m².

The evaporation of cryogenic fluids is governed by the heat conduction from the ground into the liquid pool. The solution of the one-dimensional heat conduction equation gives for the LH2 evaporation rate in kg/s:

$$dm_{LH2}/dt = A\, k\, \Delta T / [\Delta h_{fg}\, (\pi\, \alpha\, t)^{1/2}] \quad (7)$$

With A being the pool surface (in m²), k the thermal conductivity of the ground (W/mK), ΔT the temperature difference between boiling temperature of the liquid and the environment (K), Δh_{fg} the heat of LH2 vaporization (J/g), α the thermal diffusivity of the ground (m²/s), and t the time for the coverage of the ground with the liquid pool (= experimental time - 500 s). The experimental data follow the $t^{-1/2}$ dependence of the model quite well.

Thermal properties of cold concrete

The thermal conductivity k and the thermal diffusion coefficient α of concrete in Eq. (7) are temperature dependent. Furthermore, k depends also significantly on the moisture content of the concrete, which is unknown and causes the main uncertainty (± 30%) in Eq. (7).

The thermal diffusion coefficient of concrete is evaluated from the thermo-couple signals as

$\alpha = 2.5 \cdot 10^{-7}$ m²/s (8)

The average temperature drop of concrete can be estimated from the mass of vaporized LH2 at the end of the experiment:

$\Delta T = m_{LH2}\, \Delta h_{fg} / (V\, \rho\, c_p)_{concr} \approx 60$ K (9)

Take k = 2 W/mK and $\alpha = 2.5 \cdot 10^{-7}$ m²/s for calculation of the LH2 vaporization rate with Eq. (7).

Regimes in pool boiling

Pool boiling refers to boiling under natural convection conditions, in contrast to forced flow boiling. **Fehler! Verweisquelle konnte nicht gefunden werden.** shows how the boiling regime in pool boiling depends on the wall superheat*. The wall superheat ΔT_{sat} is defined as the difference between the wall temperature and the saturation temperature of the liquid at the system pressure (for LH2 T_{sat} is 20.7 K at 0.1 MPa)

$\Delta T_{sat} = T_{wall} - T_{sat}$ (10)

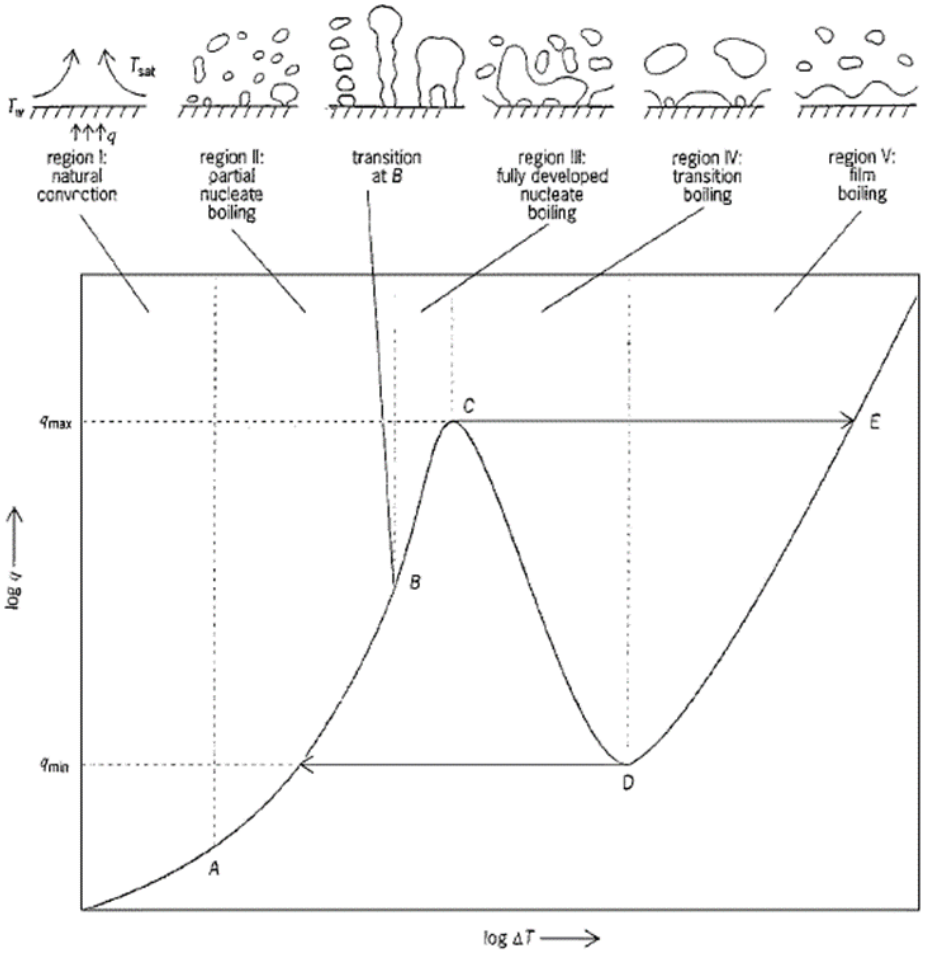

Figure 27: Boiling regimes in pool boiling versus wall superheat [3].

The section B-C represents fully developed nucleate boiling, in which the bubbles at a given site begin to merge in vertical direction. The heat flux on polished surfaces varies according to $q \sim \Delta T_{sat}^{m}$, where m has a value of 3 to 4. At point C the maximum heat flux

q_{max} (or critical heat flux CHF) sets an upper limit for heat transfer. For higher ΔT_{sat} the heater surface stabilizes rapidly at point E. In this film boiling regime the heater surface is covered with a vapor film and the liquid does not contact the solid. Heat transfer is by conduction and radiation across the vapor blanket.

Boiling regimes in the LH2 **pool vaporization tests**

The boiling heat transfer from a flat horizontal plate in LH2 has been measured by Shirai and coworkers [4]. The heat transfer under saturated condition shows a nucleate boiling regime until the critical heat flux (CHF) of 120 kW/m² is reached for $\Delta T_{sat} > 4$ K.

In the present pool experiment the heat flux from the concrete into the LH2 pool can be estimated from the measured LH2 mass loss rates dm_{LH2}/dt during the four vaporization phases (no feeding of LH2):

$$q = (dm_{LH2}/dt) \cdot \Delta h_{fg}/A \quad (11)$$

with Δh_{fg} being the heat of vaporization, and A the pool surface.

The resulting heat fluxes decrease from 27 kW/m² (≈ 200 s after begin of the experiment) to 17 kW/m² (at ≈ 740 s), which is in the nucleate boiling regime (see red dashed line in Figure 28**Fehler! Verweisquelle konnte nicht gefunden werden.**).

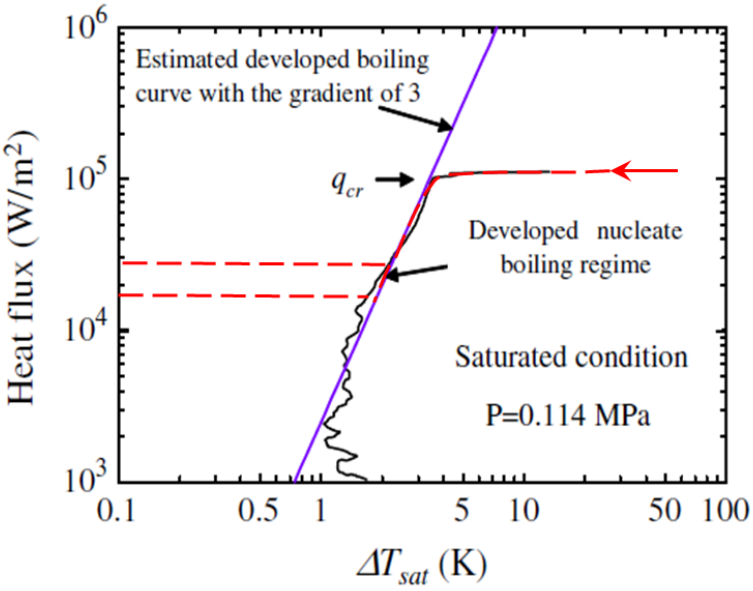

Figure 28: Heat transfer curve for P = 0.114 MPa under saturated condition with added red line for current experiments.

In the present experiment ΔT_{sat} is initially about 262 K, and the critical heat flux should be established at the concrete surface. It is expected that with increasing time and cooling of the concrete surface the heat flux follows the red line in **Fehler! Verweisquelle konnte nicht gefunden werden.**. After the concrete surface has cooled down to about 23 K a nucleate boiling regime is probably established for the rest of the experiment, as shown by the observed average density of the boiling pool calculated above.

Critical heat flux in LH2 **pool boiling**

The theoretical solution for the LH2evaporation rate predicts $dm_{LH2}/dt \rightarrow \infty$ for $t \rightarrow 0$, which is unphysical. In reality the heat transfer under saturated condition shows a nucleate boiling regime until the critical heat flux (CHF) of 120 kW/m² is reached for $\Delta T_{sat} > 4$ K [4].

In the present experiment ΔT_{sat} is initially about 262 K, and only after the concrete surface has cooled down to about 23 K the nucleate boiling regime is established. The CHF limits the maximum possible evaporation rate to:

$$(dm/dt)_{max} = A_{pool} \cdot CHF/\Delta h_{fg} = 66.8 \text{ g/s} \quad (12)$$

Eq. (7) predicts this value for t = 24.1 s. The adapted relation for the LH2 vaporization rate in the pool test is then

$$dm/dt = 66.8 \text{ g/s} \quad (t < 24.1 \text{ s}) \quad (13)$$

$$dm/dt = A\, t^{-1/2} \quad (t > 24.1 \text{ s}) \quad (14)$$

with A = 328 g/s$^{1/2}$.

In corresponding publications[1] the critical heat flux in LH2 was only measured up to $\Delta T_{sat} \approx 10$ K, while in the present concrete- LH2 pool tests ΔT_{sat} is initially 282K – 20 K = 262 K. Interestingly, the CHF for such large ΔT_{sat} was measured for horizontal platinum wires in liquid nitrogen [5].

The data show:

a) only a slight increase of the CHF (called q_{max}) with increasing ΔT_{sat},
b) a quite similar CHF value at the end of the nucleate boiling regime compared to LH2 (200 vs. 120 kW/m²)

For the pool tests with LH2 on concrete it may be expected that the CHF is initially somewhat larger than 120 kW/m², but it rapidly approaches this value as the concrete surface is cooled down to about 25 K.

Calculated vaporized LH2 **mass**

The total vaporized LH2 mass in the pool test $m_{LH2}(t)$ can be estimated from the integration of the vaporization rate given in Eq. 15:

$$m_{LH2}(t) = B \cdot t \quad (t < 24.11 \text{ s}) \text{ with } B = 66.81 \text{ g/s} \quad (15a)$$

$$m_{LH2}(t) = 2A\, t^{1/2} + C \quad (t > 24.11 \text{ s}) \text{ with } A = 328 \text{ g/s}^{1/2} \text{ and } C = -1610 \text{ g} \quad (15b)$$

The results are plotted in Figure 29. The plot shows

a) the initial linear part of Eq. (15) due to the CHF limitation (valid up to 24.11 s), and
b) the succeeding $t^{1/2}$ dependence due to the decreasing heat transfer rate from the concrete,
c) after 800 s (the end of the test = 1300 – 500 s) about 17 kg of LH2 have vaporized.

[1] Y. Shirai et al, Boiling heat transfer from a horizontal flat plate in a pool of liquid hydrogen, Cryogenics 50 (2010) 410-416

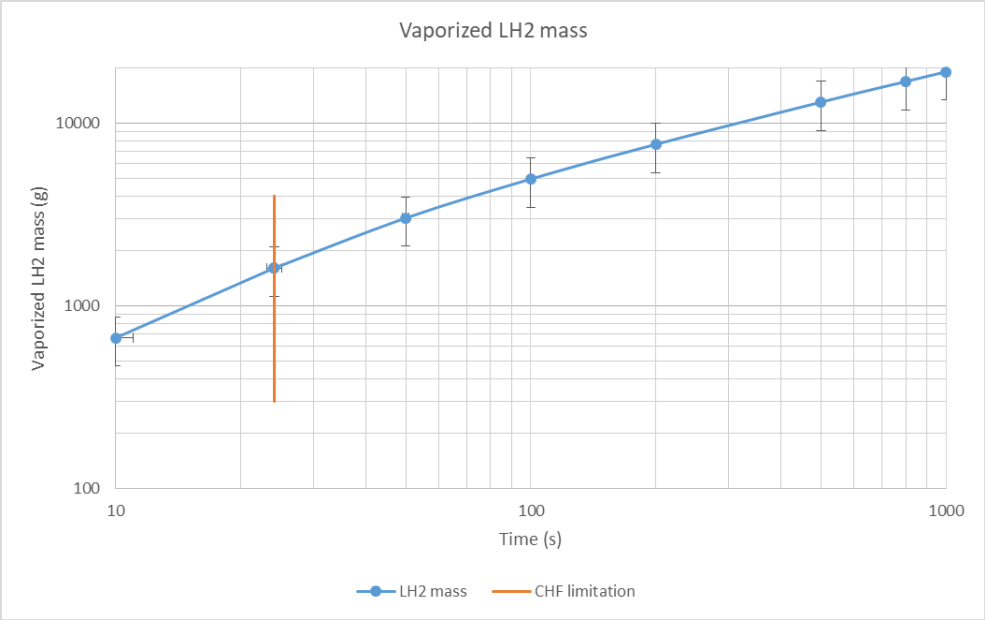

Figure 29: Vaporized LH2 mass versus time.

Ground thermocouples

Thermocouples (TC) were used to measure the transient heat transfer from the concrete to the LH2 pool. They were installed at five different distances to the concrete surface. The TC signals react to two short dry-out periods of the LH2 pool beginning at about 720 and 1080 s (**Fehler! Verweisquelle konnte nicht gefunden werden.**). The pool dried out at 1300 s due to stop of LH2 supply. The first five TC in the legend (with designations -00) are installed on the central vertical axis of the concrete slab. At the 14 mm distance to the upper surface three thermocouples are located in a horizontal plane (TG86-00, TG86-05 and TG86-15). Their signals are quite close to each other, showing that the heat transfer is essentially one-dimensional in vertical direction. The measured temperatures were also plotted at four different times as function of the distance from the concrete surface (Figure 30).

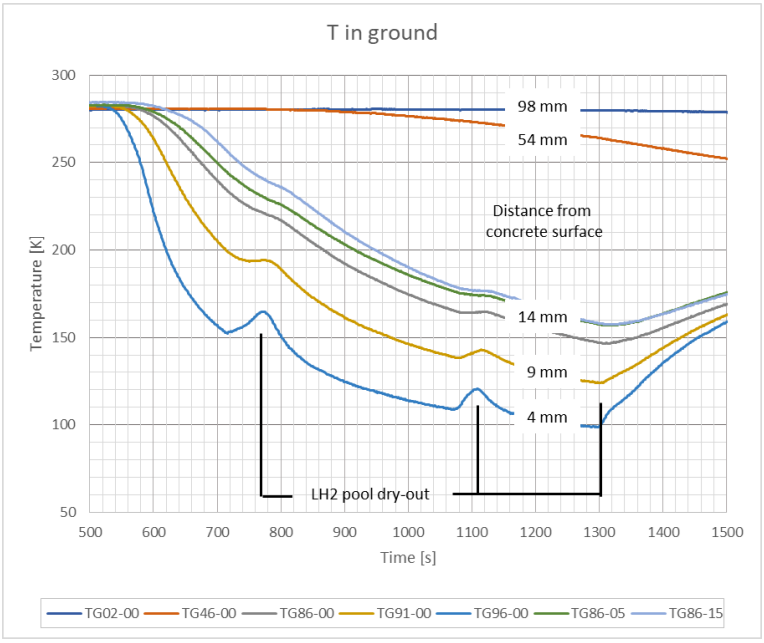

Figure 30: Temperature courses of the ground thermocouples in experiment 20200423-Concrete02.

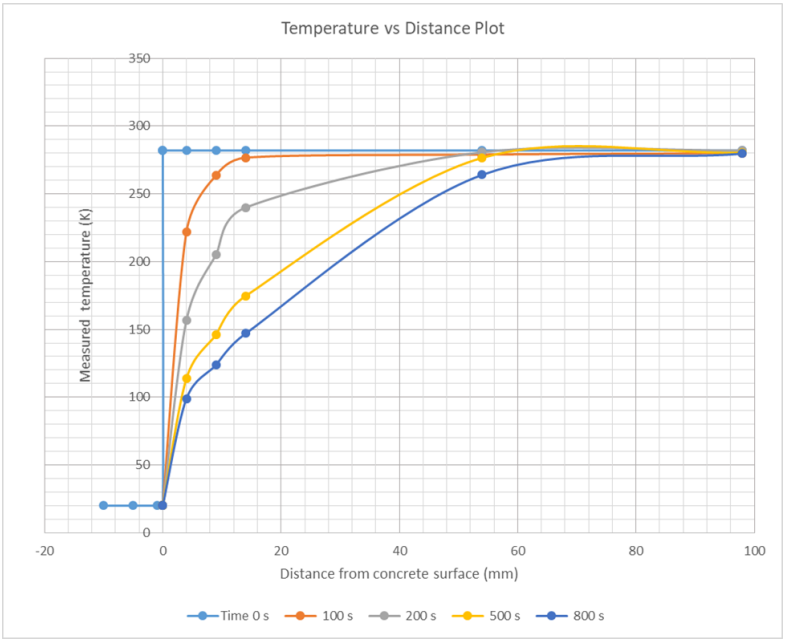

Figure 31: Measured temperatures versus distance from the upper concrete surface in experiment 20200423-Concrete02.

Figure 31 shows measured temperatures versus distance from the concrete surface for four different times. Zero point for this time scale is 500 s of the experimental time (see Figure 30). Added is the (ideal) initial temperature of the concrete slab (20 K at surface, 282 K inside). The temperature data in this format show how the cooling wave progresses from the surface into the interior of the concrete.

The straight lines between 0 and 4 mm are assumed extrapolated temperatures to 20 K, they are not measured. The wavy structure near the 9 mm position (TC TG91-00) would

be reduced if this TC was installed at 7 mm instead of the nominal 9 mm distance to the surface, which is within the experimental uncertainty.

Enthalpy loss from concrete due to LH2 vaporization

The enthalpy loss from the concrete should correspond to the mass of vaporized LH2. The concrete enthalpy loss is

$$\Delta H = \rho\, cp\, A \int_{x=0}^{x=x_{end}} (T_0 - T(x))\, dx = \rho\, cp\, A\, [T_0\, x_{end} - \int_{x=0}^{x=x_{end}} T(x)\, dx] \quad (16)$$

The term in the square bracket corresponds to the blue area in the left drawing of Figure 31 (case t = 100 s). The hydrogen mass which can be evaporated with this enthalpy change of the concrete ΔH is

$$m_{LH2} = \Delta H / \Delta h_{fg} \quad (17)$$

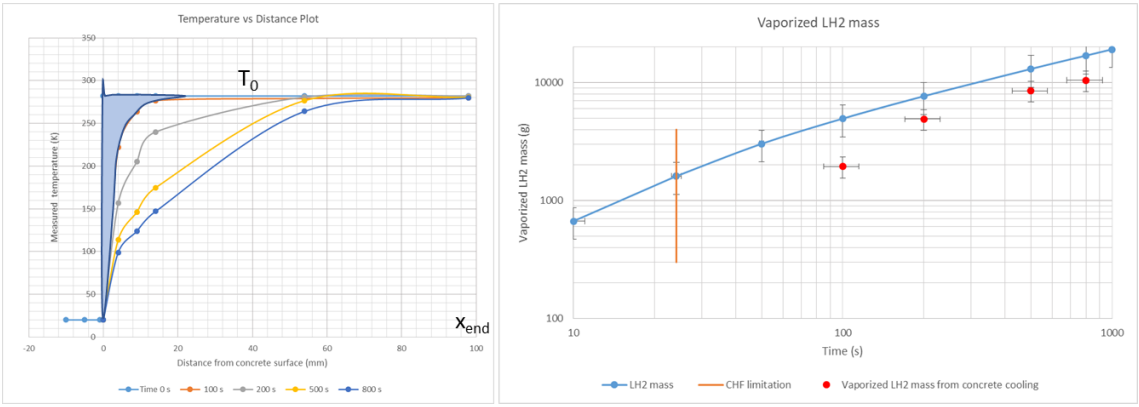

Figure 32: Measured temperatures versus distance (left) and vaporized LH2 mass (right).

The values for this mass are shown in the right graph of Figure 32 as red points for the times 100, 200, 500, and 800 s. The last three points agree within the uncertainties with the vaporized LH2 masses of Eq. (15). This integral energy balance shows that the TC data are fairly consistent with calculated masses of evaporated LH2 (the value at t = 100 s is too low because a stable liquid pool was not yet established for t < 100 s, the surface temperature of the concrete was above 20 K).

5 Experiments E3.5 – RAIN-OUT tests

The main objective of this series of experiments was to investigate the propensity for rainout to occur when LH2 is released from elevated positions. This included vaporisation, the characterisation of the flow at the point of release and the subsequent dispersion of the gaseous hydrogen cloud. The capacity for these releases to form pools was also explored.

To meet these objectives, a series of 25 unignited LH2 releases was carried out through 6 mm, 12 mm, and 25.4 mm nozzles with an indicated tanker delivery pressure of 0.1 or 0.5 MPa and release heights of 0.5 m or 1.5 m. The dispersion from these releases was measured in terms of hydrogen concentration and temperature. Other attributes such as pressure, mass flow rate and temperature were measured in the pipework to provide an understanding of the source term. As well as these measurements, multiple videos were taken of each release including; thermal, high speed and drone footage.

The testing was carried out using the LH2 release facility, located on a 32 m diameter concrete pad at the Frith Valley site at the HSE Science and Research Centre in Buxton.

While no evidence of rainout was found during these releases, evidence of rainout immediately after a release was observed. Further to this, condensed components of air formed around the release point and on impingements. Pools were only formed with low, vertically downward releases. These pools potentially comprised of LH2, condensed components of air, or a mixture of the two. It is possible that with different initial conditions or obstruction geometries, rainout and pool formation could still occur.

The phase of hydrogen at the release point was indicated by the pipework measurements. For the majority of the trials a two-phase flow developed within the release pipework. This has been attributed predominantly to the heat transfer into the fluid in the final 3 m of pipework, which contained the instrumentation and therefore was not vacuum insulated. The mass flow rate for each source configuration was measured and is reported including the methodology.

The development and dispersion of the gaseous H2 cloud that forms from a release of LH2 was captured by the instrumentation and video footage. The jet is typically momentum dominated for the initial section, which ranges between 1.5 m and 6 m depending on the release pressure and nozzle size, but then becomes extremely dependent on the wind, including transient localised gusts.

The video and data output of these experiments are provided for model validation on the KITOpen repository.

5.1 Rain-out test facility

The experiments were conducted using the LH2 release facility, which was located on a 32 m diameter concrete pad at the Frith Valley site at the HSE Science and Research Centre in Buxton.

The experiments relied on four main components, shown in Figure 33: the LH2 release station in the centre, the tanker and vent stack in the bottom right, the near-field array just on the left of the centre, and the far-field stands on the far left of the concrete pad.

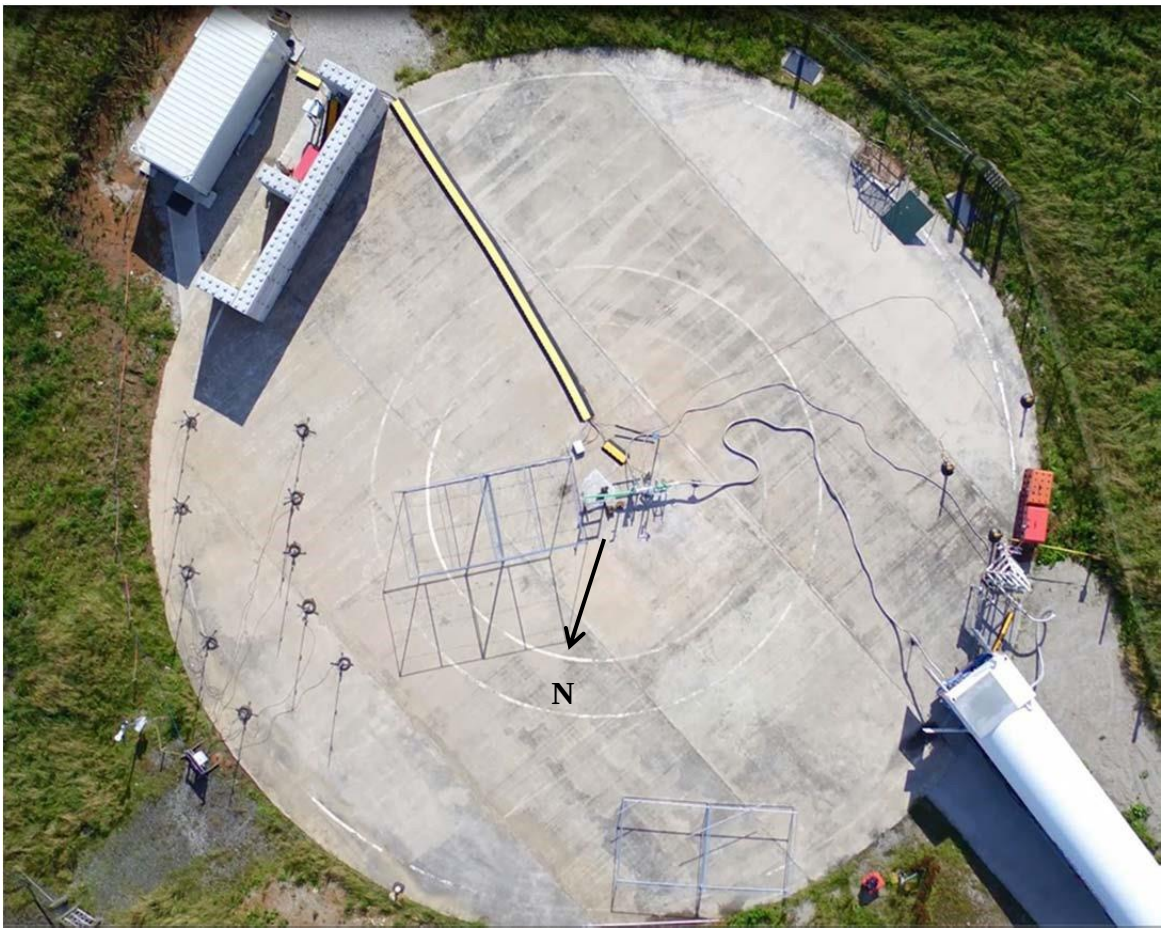

Figure 33: Still image from drone footage

5.1.1 Release station

The release station as shown in Figure 34 encompassed the pipework and valves required to operate the system remotely as well as instrumentation to characterise the flow of LH2. For these tests this consisted of an electrically isolated pipe section, a valve section and a flexible hose. The nominal bore of the pipework was a constant 25.4 mm. The instrumentation consisted of two 1 MPa Wika IS-3 pressure transducers, four type T thermocouples and a Micro Motion Coriolis mass flow meter with an Elite 5700 transmitter. A PCE-FWS-20 weather station was mounted nearby. The mass flow meter was modified by the manufacturer to help facilitate operation at temperatures below 70 K. A 20 m, 25.4 mm nominal bore vacuum insulated hose connected the release station to the tanker and a mixture of foam, aluminium tape and insulation tape covered the remaining parts.

Figure 34: Photo of release station.

The distances from each sensor in the pipework to the release point and dimensions of the pipe sections, including the approximate R values for the insulation, are available in the experiment description on the KITOpen repository.

5.1.2 Tanker and vent stack

The LH2 was supplied by Air Liquide in a vacuum insulated tanker, which could hold up to 2.5 tonnes. Control of the pressure and conditioning of the LH2 inside the tanker was achieved through venting the ullage of hydrogen gas to lower the pressure, or allowing LH2 into a heat exchanger underneath the tanker to raise the pressure. A 1.2 MPa bursting disk protected the tanker against over pressurisation.

The tanker was connected to the release pipework, 3 m vent stack and valve control system. The instrumentation on the tanker was not logged, but the pressure was recorded for each trial from the dial gauge on the tanker. One type T thermocouple was installed on the lower face of the vent stack exit. Figure 35 shows the tanker connected to the vent stack. The N_2 and H_2 gas cylinders shown in the photo were used to purge the pipework of air prior to each release.

Figure 35: Photo of tanker, vent stack, and purging station.

5.2 Instrumentation, Measurement equipment

To capture the hydrogen concentration of the jet formed by a release of LH2, an array supporting 31 sampling tube lines and 24 type T thermocouples was placed downstream of the release point. Each thermocouple was collocated with a sampling line. The sampling lines were 1/8” diameter and 30 m long, which resulted in a delay of approximately 18 s for the sampled gas to reach the hydrogen sensors. The sensors, which were Xensor thermal conductivity sensors, were supplied by the National Renewable Energy Laboratory (NREL) for these tests. The release station and near-field array were oriented with the prevailing wind direction. For these tests the nozzle was pointing approximately eastwards as the dominant wind direction came from the West (270° from North). Figure 4 shows the near-field array ready for a release at 1.5 m. Releases were carried out at 0.5 m and 1.5 m above the ground and varied in orientation, i.e. upward, downward and horizontally.

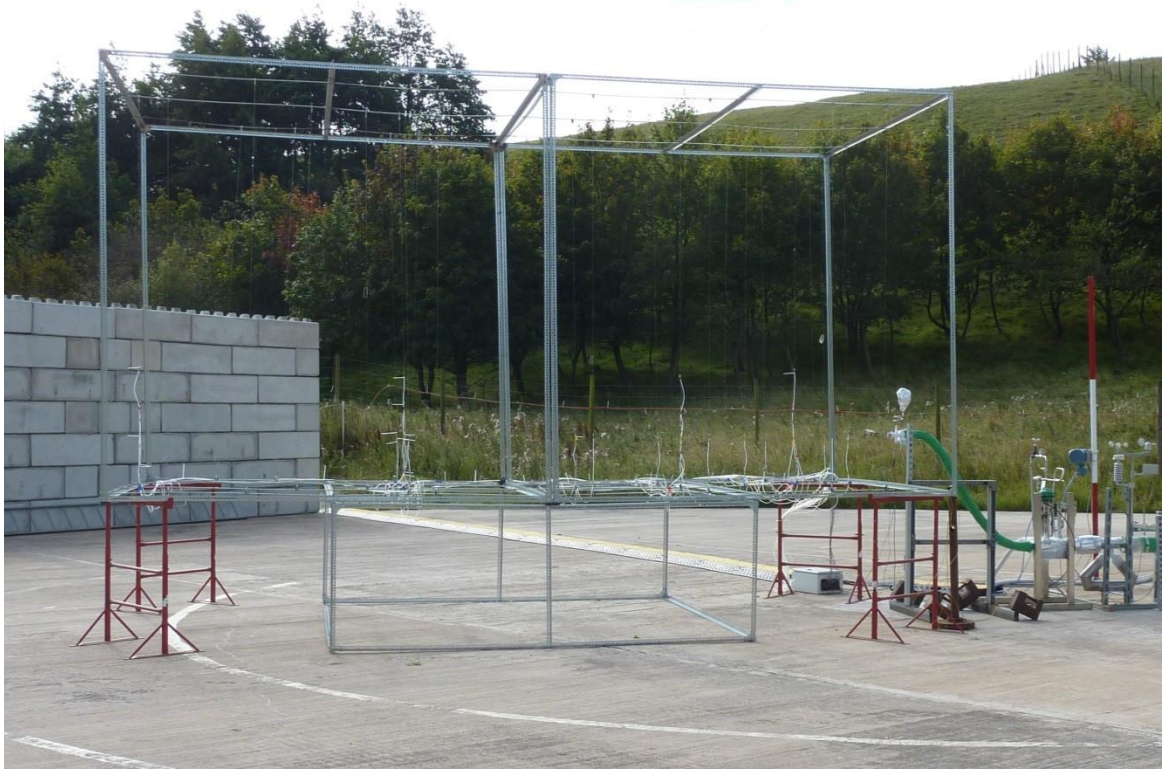

Figure 36: Photo of near-field array configured for releases at 1.5 m height.

Further downstream of a release of LH2, the jet develops into a cloud. To observe this downstream behavior 10 mobile stands, each with three Dräger Xam 5000 personal gas detection devices and collocated type T thermocouples, were arranged in the expected dispersion path. The Dräger devices each contained four sensors: hydrogen ppm, hydrogen %Vol, hydrogen %LEL and oxygen depletion. The release station was orientated in line with the dominant wind direction. Due to varying wind conditions, some trials were carried out with an alternate stand layout. Figure 37 shows a photograph of the sensors in the standard positions.

Figure 37: Photo of far-field stands.

Weather data was collected at two locations: on a 3 m high stand on the downwind edge of the concrete pad approximately 20 m from the release point, and locally to the release station at 1.5 m height.

Video footage was recorded for each trial by a selection of the following cameras: three Sony FDR-AX53 handy cams recording at 50 fps provided standard footage with three views; a high speed Phantom Mira LC320 recording at 3600 fps captured detailed footage of the release point; a FLIR X8400sc thermal camera indicated the extent of the cold gas; and a drone-mounted DJI X5R recording at 25 fps showed the direction of the gas cloud, including the effect of the wind on the downstream plume.

Various acquisition systems were used to collect the data from the instruments. The primary system not only logged but also controlled the remotely operated valves. Each logging PC was networked and therefore shared a common time-base..

The primary method of acquisition and valve control was running on a dedicated PC with Flexlogger. Various National Instruments chassis and logging cards were used to collect data from the range of sensors. Each thermocouple and pressure transducer was logged through this system, as was the far-field weather station, which recorded humidity, wind speed and wind direction. The mass flow meter was also connected to the primary acquisition system. Logging was enabled before each test at a rate of 1 Hz.

The near-field gas sensors were connected to two PCs via USB hubs and continuously logged at 4 Hz in a bespoke LabVIEW program, written by NREL. Pumps drew gas

through approximately 30 m of tubing, giving a delay of approximately 18 seconds. Each sensor produced its own output text file, which were then compiled into a single table for each test.

Each far-field gas concentration measurement device (Dräger Xam 5000) was a standalone logger and sensor, logging at 1 Hz. The far-field concentration sensors were logged continuously during each test day. Each sensor was synchronised onto a common timebase and collated into a single table for each test.

As well as being connected to the primary logging system, the mass flow meter was connected directly to a secondary PC running the manufacturer's logging software. The mass flow meter was logged continuously during each test day. The data was downloaded as a table and synchronised to the common timebase.

The average weather conditions at the release point were logged once per 5 minutes on a separate system. The local weather station on the release point logged for the duration of each test day.

5.2.1 Estimate of measurement errors

The accuracy data of the sensors used in the experiment are summarized in Table 11. The information is taken from the respective manuals for the equipment. There are additional uncertainties in the use of the thermocouples and the flow meter at cryogenic temperatures. The inherent variability in conducting experiments outdoors needs to be taken into consideration when interpreting the results.

Table 11: Accuracies of sensors.

Sensor	Manufacturer	Model	Range	Accuracy
Pipework thermocouples	TC Direct	1.5 mm Type T Mineral insulated	–200 to 350°C	±1.5% of Reading
Near-field thermocouples	TC Direct	1.5 mm Type T Mineral insulated	–200 to 350°C	±1.5% of Reading
Far-field thermocouples	TC Direct	1.5 mm Type T Grounded Chamfered tip	–200 to 350°C	±1.5% of Reading
Pressure	Wika	IS-3	0-10 barg	±0.5% of Full Scale
Tank Pressure	N/A	Dial gauge	0-15 barg	Visual
Mass flow	Emerson	Micro Motion Coriolis meter	0-7.5 kg/s	±3% of Reading*

H2 concentration	Xensor	XEN-5320	0-100 Vol %	±3% of Full Scale
H2 concentration	Dräger	Xam 5000 XXSH2 HC	0-4 Vol %	±2% of Reading
H2 concentration	Dräger	Xam 5000 Cat-Ex 125	0-100% LEL	±1% of Reading
H2 PPM	Dräger	Xam 5000 XXS H2	0-2000 ppm	±1% of Reading
O2 depletion	Dräger	Xam 5000 XXS O2	0-25 Vol %	±1% of Reading
Near-field weather station	PCE Instruments	PCE-FWS-20	0-240 km/h 10-90 % humidity	Indicator
Far-field wind sensor	Gill Instruments	Windsonic	0-60 m/s 0-359°	±3% of Reading ±2°
Far-field humidity sensor	Skye Instruments	SKH 2053	0-100 % -20 to 70°C	±2% ±0.05°

* Typical accuracy of 0.1 % for liquid flow at ambient temperature, estimated accuracy of 3% at cryogenic temperatures.

5.3 Test programme

The test programme was designed to look for the occurrence of LH2 rainout and in its absence to provide data on the release and dispersion. To achieve this, a series of experiments changing the release height, release orientation, tanker pressure and nozzle size were planned. Table 12 shows the resulting experimental plan.

Table 12: Experimental plan of the Rain-out tests

Test No	Release Orientation	Release Height Above Ground (m)	Orifice Diameter (mm)	Pressure (barg)
3.5.1	Horizontal	0.5	25.4	1
3.5.2	Horizontal	0.5	12	1
3.5.3	Horizontal	0.5	6	1
3.5.4	Horizontal	1.5	25.4	1
3.5.5	Horizontal	1.5	12	1
3.5.6	Horizontal	1.5	6	1
3.5.7	Vertical Up	0.5	12	1
3.5.8	Vertical Down	0.5	12	1
3.5.9	Horizontal + obstruction	0.5	12	1
3.5.10	Horizontal	0.5	25.4	5
3.5.11	Horizontal	0.5	12	5
3.5.12	Horizontal	0.5	6	5
3.5.13	Horizontal	1.5	25.4	5
3.5.14	Horizontal	1.5	12	5
3.5.15	Horizontal	1.5	6	5
3.5.16	Vertical Up	0.5	12	5
3.5.17	Vertical Down	0.5	12	5
3.5.18	Horizontal + obstruction	0.5	12	5

Over time, a portion of the LH2 vaporises in the tank and a head of gaseous hydrogen forms, building the pressure. This subsequently increases the boiling point of the fluid in the tanker, increasing the likelihood of flashing in the pipework. Prior to each day of testing, the pressure was reduced to atmospheric pressure by releasing some of the hydrogen gas. It was then raised to the pressure required in the trials. This was completed by allowing LH2 from the bottom of the tank into the heat exchanger, where vaporisation occurs. The gas was then fed back into the top of the tank.

Air in pipework with LH2 poses significant hazards, as there is the potential to form both blockages and flammable mixtures. As such, immediately before each set of releases the pipework was purged; firstly with nitrogen, then with ambient hydrogen gas. Once the purge was complete, LH2 could be introduced to the pipework.

Recording was initiated and the main release valves opened. Each experimental release lasted between 2-10 minutes with the aim of achieving a steady state output from the temperature sensors within the pipework and the flow meter. If the wind speed or direction proved unfavourable, the test was stopped. Upon completion, the main release valves were closed and the vent line opened, allowing any LH2 remaining in the pipework to vaporise and disperse safely.

5.4 Results

A series of 25 unignited LH2 releases were carried out through 6 mm, 12 mm, and 25.4 mm nozzles with an indicated tanker pressure of 0.1 or 0.5 MPag and release heights of 0.5 m or 1.5 m. Table 13 shows the trials and data gathered. Standard and high-speed footage was captured for each trial.

Table 13: Instrumentation notes and cameras per trial.

Trial No	Test No	Initial conditions	Footage	Notes
1	3.5.3	6 mm, 1 barg	Standard, drone & thermal	Scoping trial.
2	3.5.1	25.4 mm, 1 barg	Standard, drone & thermal	Scoping trial.
3	3.5.1	25.4 mm, 1 barg	Standard, drone, thermal & high-speed	1 Dräger device non-functional.[2] Stand 9 medium TC non-functional.
4	3.5.2	12 mm, 1 barg	Standard, drone, thermal & high-speed	11 Dräger devices non-functional. Stand 9 medium TC non-functional.

[2] The Dräger devices were non-functional for some tests due to the battery running out. This was primarily caused by the non-standard use of the devices for these trials resulting in extended alarming periods.

5	3.5.3	6 mm, 1 barg	Standard, thermal & highspeed	1 Dräger device non-functional, Stand 9 medium TC non-functional.
6	3.5.7	12 mm, 1 barg	Standard	1 Dräger device non-functional. Stand 9 medium TC non-functional.
7	3.5.8	12 mm, 1 barg	Standard & thermal	1 Dräger device non-functional. Stand 9 medium TC non-functional.
8	3.5.8	12 mm, 1 barg	Standard, thermal & highspeed	All functional.
9	3.5.9	12 mm, 1 barg	Standard, drone, thermal, high-speed	All functional.
10	3.5.10	25.4 mm, 5 barg	Standard, drone, thermal, high-speed	First 4 near-field centreline sampling lines become blocked during the test.
11	3.5.11	12 mm, 5 barg	Standard, drone, thermal, high-speed	1 Dräger device non-functional. First 3 near-field centreline sampling lines become blocked during the test.
12	3.5.12	6 mm, 5 barg	Standard, drone & thermal	2 Dräger devices non-functional.
13	3.5.17	12 mm, 5 barg	Standard, drone, thermal, high-speed	2 Dräger devices non-functional.
14	3.5.16	12 mm, 5 barg	Standard, drone & thermal	2 Dräger devices non-functional.
15	3.5.18	12 mm, 5 barg	Standard, drone, thermal, high-speed	3 Dräger devices non-functional.
16	3.5.4	25.4 mm, 1 barg	Standard, drone & highspeed	Far-field weather station non-functional.
17	3.5.5	12 mm, 1 barg	Standard, drone & highspeed	Far-field weather station non-functional.
18	3.5.6	6 mm, 1 barg	Standard, drone & highspeed	Far-field weather station non-functional.
19	3.5.4	25.4 mm, 1 barg	Standard & drone	Far-field weather station non-functional.

20	3.5.5	12 mm, 1 barg	Standard & drone	Far-field weather station non-functional.
21	3.5.6	6 mm, 1 barg	Standard & drone	1 Dräger device non-functional. Far-field weather station non-functional.
22	3.5.13	25.4 mm, 5 barg	Standard & drone	1 Dräger device non-functional. Far-field weather station non-functional. First 4 near-field centreline sampling lines become blocked during the test.
23	3.5.14	12 mm, 5 barg	Standard & drone	2 Dräger devices non-functional. Farfield weather station non-functional. First 3 near-field centreline sampling lines become blocked during the test.
24	3.5.15	6 mm, 5 barg	Standard & drone	2 Dräger devices non-functional.
25	3.5.13	25.4 mm, 5 barg	Standard & drone	3 Dräger devices non-functional. First 4 near-field centreline sampling lines become blocked during the test.

One of the main objectives of the trials was to establish the propensity for droplets of LH2 to form and fall to the ground from elevated LH2 releases. However, identifying LH2 rainout rather than liquid air remains an ever present challenge to measure with instrumentation. Close-up footage of the experiments provides an indication of the phenomenon but not its composition.

For un-impinged elevated releases, no evidence of rainout was observed during the releases. However, in some circumstances condensates occurred. Droplets formed and fell to the ground immediately after the main release valve was closed on some trials; solid build-up on the nozzle at the release point was present when using the 12 mm or 6 mm nozzles; pools formed from low, vertically downwards releases; and solid deposits formed on the nearest sensors in the high-pressure streams.

The possibility of rainout occurring at the top of the vent stack during a venting operation was also explored, however the temperature did not fall below approximately -190°C throughout the entire experimental series.

Although it is unclear if this was a consistent phenomenon due to the difficulty in classification, trial 10, which was a high pressure release through the 25.4 mm nozzle, displays rainout immediately after the main release valve is closed. No pool forms as the droplets hit the ground as they appear to evaporate rapidly. Figure 38 and 39 display this process.

Figure 38: Droplets forming as the main stream loses momentum.

Figure 39: Droplets hitting the ground and rapidly evaporating.

Throughout the series of experiments, releases through the 12 mm and 6 mm consistently formed white cone deposits at the release point. Evidence of the formations altering the jet was also observed, including an example of the jet becoming two separate streams, shown in Figure 8. These formations would form and break off periodically throughout a release.

When conducting the 'high pressure' releases, with the tanker pressure at 0.5 MPa, the LH2 jet interacted with the closest sampling lines of the near-field sensors. Large solid deposits formed, blocking the sampling tubes and distorting the jet. Periodically, part of this formation would dislodge and fall to the floor, where it appeared to sublime. Figure 40 shows a set of stills of this process taken from trial 10.

Figure 40: A solid deposit on the nearest sampling line (left) and part of the solid deposit on the ground (right).

Pools did not form for the majority of the trials, but for trials 7 and 8, which were oriented vertically downwards, pools of approximately 1.7 m diameter formed. This was evidenced by frost marks on the concrete following the tests and the video captured during the trials, although this was heavily obscured due to the formation of mist. No rainout or pools were formed from vertically upwards releases and, due to the physical layout of experiments, the majority of the hydrogen plume did not interact with the sensors.

5.4.1 Measurements in the pipework

The pipework pressure was measured at two points, one before the main release valve and one at the nozzle. When conducting a trial the valves between the reservoir of LH2 and the open atmosphere at the release point were open, allowing the tanker pressure to drive flow through the pipework.

The nozzle size had an impact on the pressures recorded in the pipework, as there is a balance between frictional losses in the pipework and losses introduced by the nozzle. Figure 41 shows example nozzle pressure readings over time for each nozzle size at 0.1 and 0.5 MPa. Trials 3-5 and 10-12 were used to illustrate the nozzle pressure behaviours.

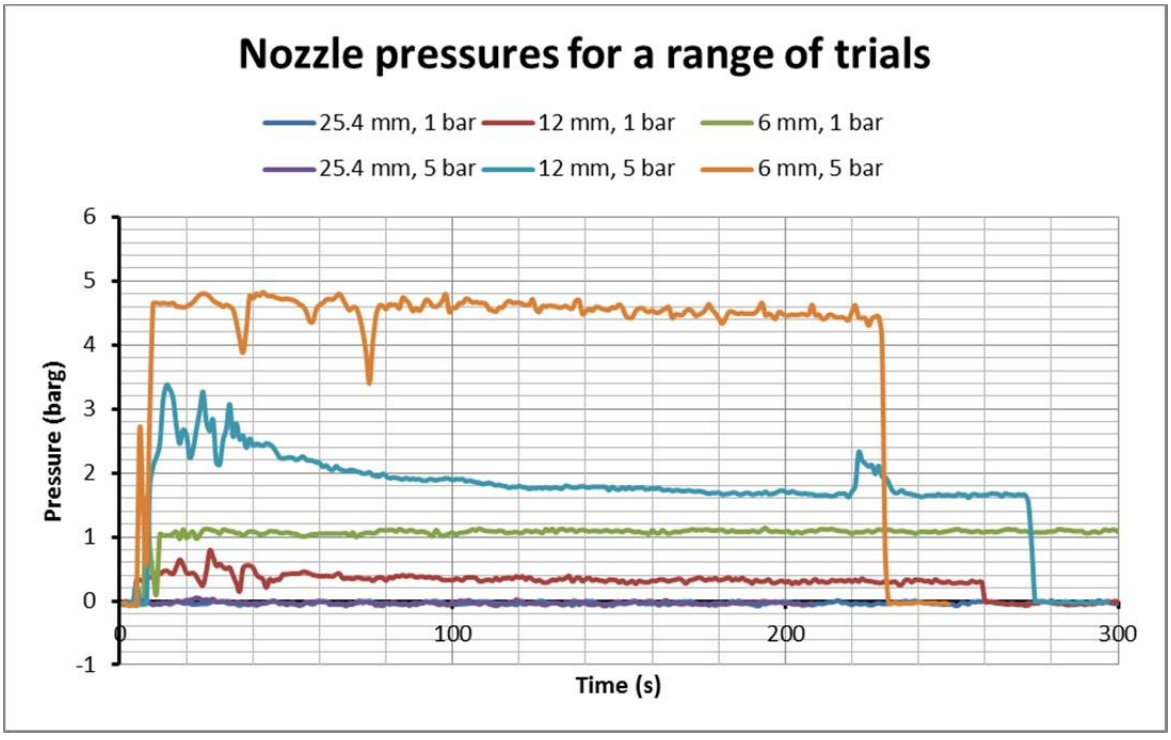

Figure 41: Recorded nozzle pressures for each nozzle at 1 and 5 barg pressure.

The pipework temperature measurements were taken to enable characterisation of the source term. Each different nozzle size and pressure combination showed different characteristics in the pipe. The temperature was measured at three points in the flow of the LH2 in the pipework, and at one point on the outer surface of the pipework. The raw data was logged in μV and was uncompensated for the cold junction temperature.

The results over each release showed three typical regions: the initial phase in which the temperature drops from ambient conditions; a phase in which the temperature continues to decrease but shows instability; and a final steady state. The regions of the graph indicate the phase state of the hydrogen.

The initial conditions of the pipework and tanker influenced the outputs of the temperature sensors. When the larger nozzles were used the rate of cooling was increased and the phase of instability shorter. When the pipework was pre-cooled by earlier tests, the drop from ambient conditions is, in some cases, not present due to the pipework being at cryogenic temperatures at the start of the trial.

The measurements, made in microvolts, were converted to temperature using the NIST type T lookup tables and reference cold junction measurements. The results for trial 5 are shown in Figure 42.

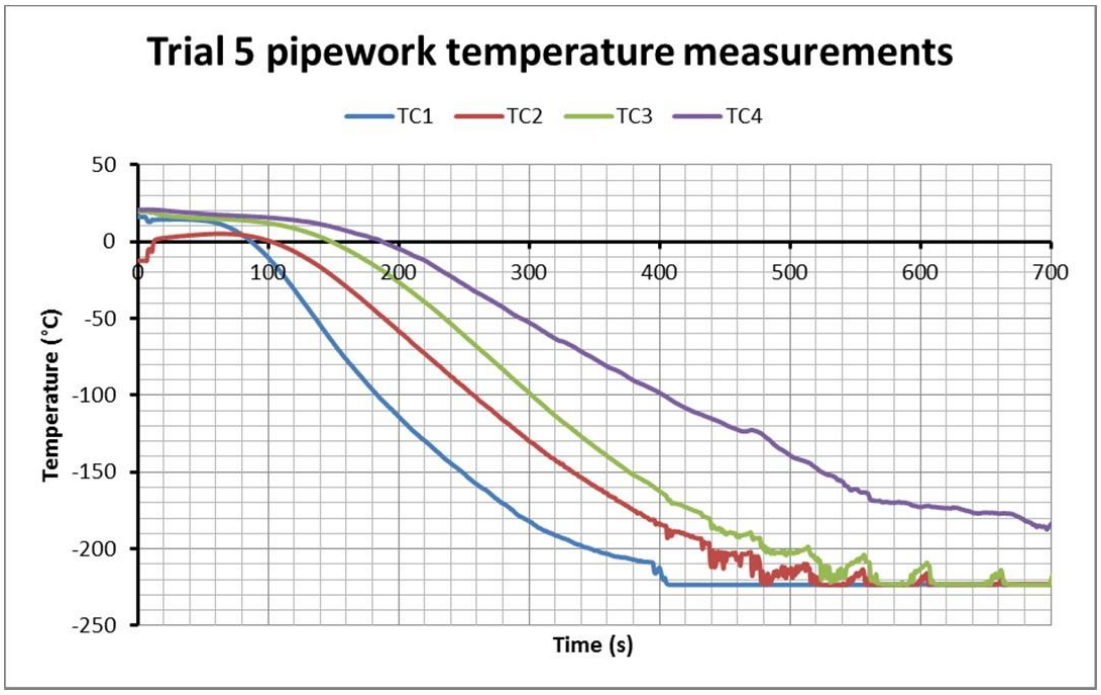

Figure 42: Graph showing trial 5 pipework temperatures.

The mass flow rates determined for the different configurations are shown in Table 14. Some values (for smaller nozzles at high pressure) are known with confidence from the mass flow meter. In other cases (low pressure and/or open pipe) the mass flow meter saw a 2-phase flow with a high void fraction and did not give reliable output. The mass flows can, however, be derived (within a range) from pressure measurements.

Table 14: Massflow rates in the PRESLHY rain-out tests

Pressure	Nozzle diameter	Mass flow
5 bar	6mm (¼ ")	90-100 g/s
5 bar	12mm (½")	265 g/s
5 bar	1" (open pipe)	298 g/s
1 bar	6mm (¼ ")	Unknown
1 bar	12mm (½")	104-107 g/s
1 bar	1" (open pipe)	135-144 g/s

One source condition, which could not be measured directly or derived, was a driving pressure of 0.1 MPa and a nozzle diameter of 6 mm. This is due to the flow being predominantly gaseous and the subsequent flow rate/pipework pressure drop being too low for the flow meter/pressure transducers to resolve. The mass flow in previous work on solid accumulation used much of the same equipment and the PRESLHY data can be used to estimate the flow rate in these experiments at approximately 135 g/s.

A detailed description of the methods used to interpret flow rate and density measurements are given in the corresponding detailed description provided on the KITOpen repository.

5.4.2 External measurements

In the near-field array, concentration and temperature measurements were made. This was to examine the dispersion of the LH2 jet axially along the centerline and radially outwards. The thermocouples and sampling lines were collocated to investigate a potential correlation between temperature and hydrogen concentration.

Each sensor output gives the concentration over time at a specific point. By averaging each point during the steady state of a release, the transient effect of the dynamic wind conditions can be mitigated and comparisons can be made between tests. Figure 43 and 44 show the average H_2 concentrations across the near-field array at 0.5 m height for different nozzle sizes and pressures. The maximum H_2 concentrations are displayed in a similar format in Appendix B.

Figures 22 and 23, marked with *, show lower than expected concentrations along the centrelines close to the release point. This is thought to have been caused by a solid formation developed on the sampling lines during high pressure trials, effectively blocking the sensor.

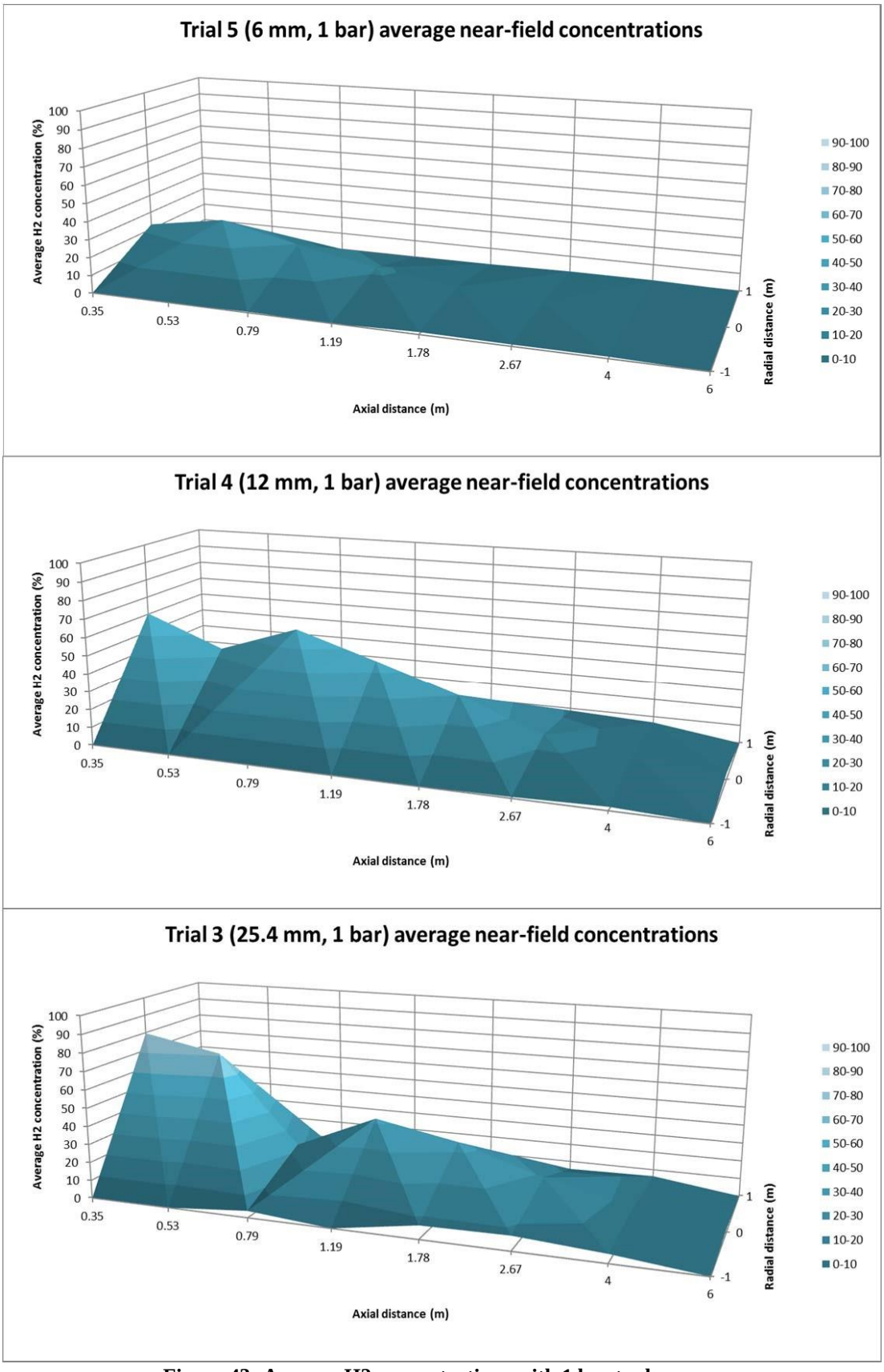

Figure 43: Average H2 concentrations with 1 bar tanker pressure.

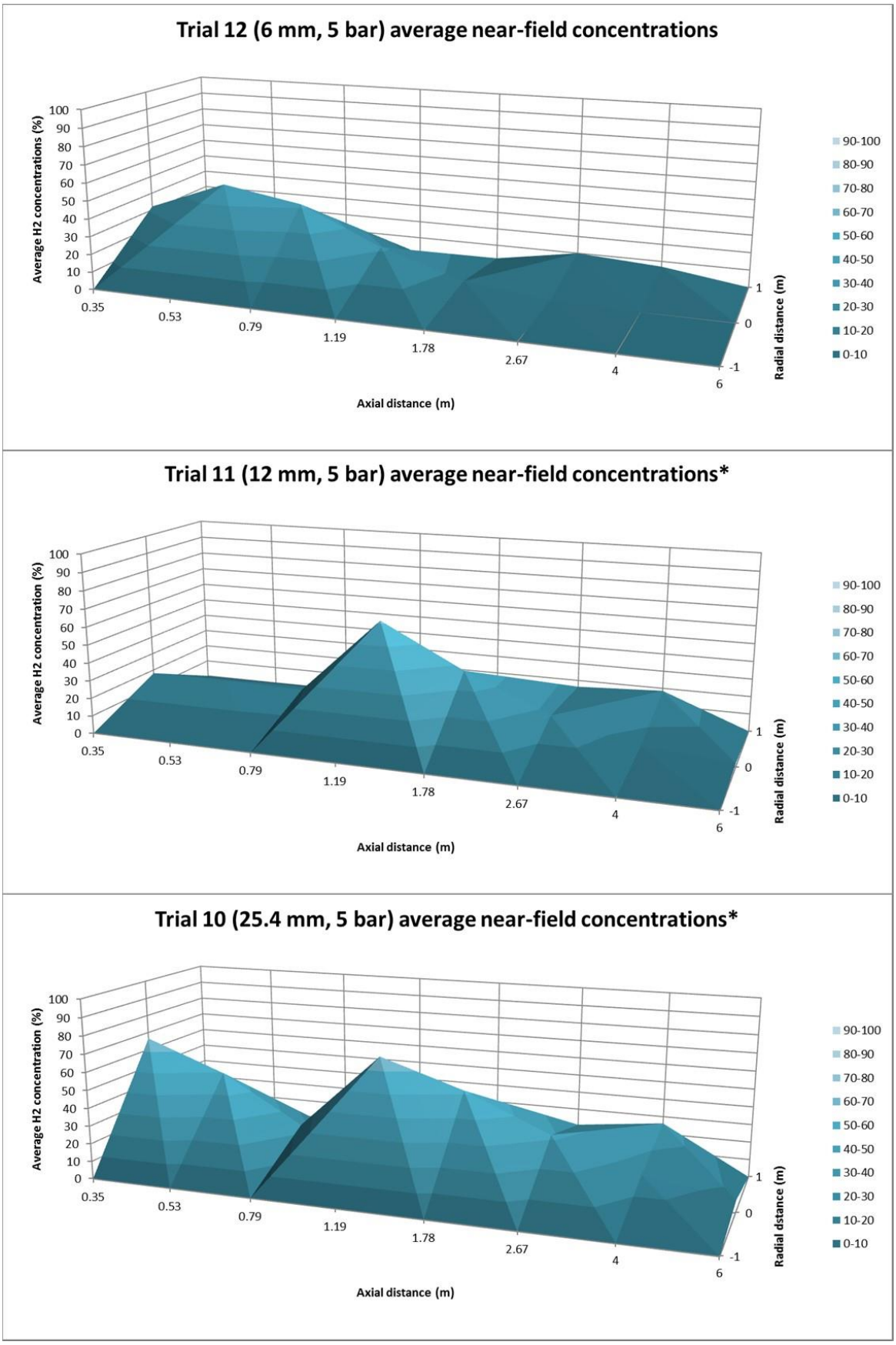

Figure 44: Average H2 concentrations with 5 bar tanker pressure.

The near-field H_2 concentration sensors were supplemented with 24 type T thermocouples, which were collocated with a selection of the sampling lines. For each test, the minimum measured temperature and maximum measured concentration at each collocated point was plotted. This can be seen in Figure 45, which is a plot of the minimum measured temperature and the maximum measured hydrogen concentration across the 24 collocated pairs in each trial. This relationship will be examined as a future part of the PRESLHY project aimed at predicting the concentration of hydrogen based on temperature measurements.

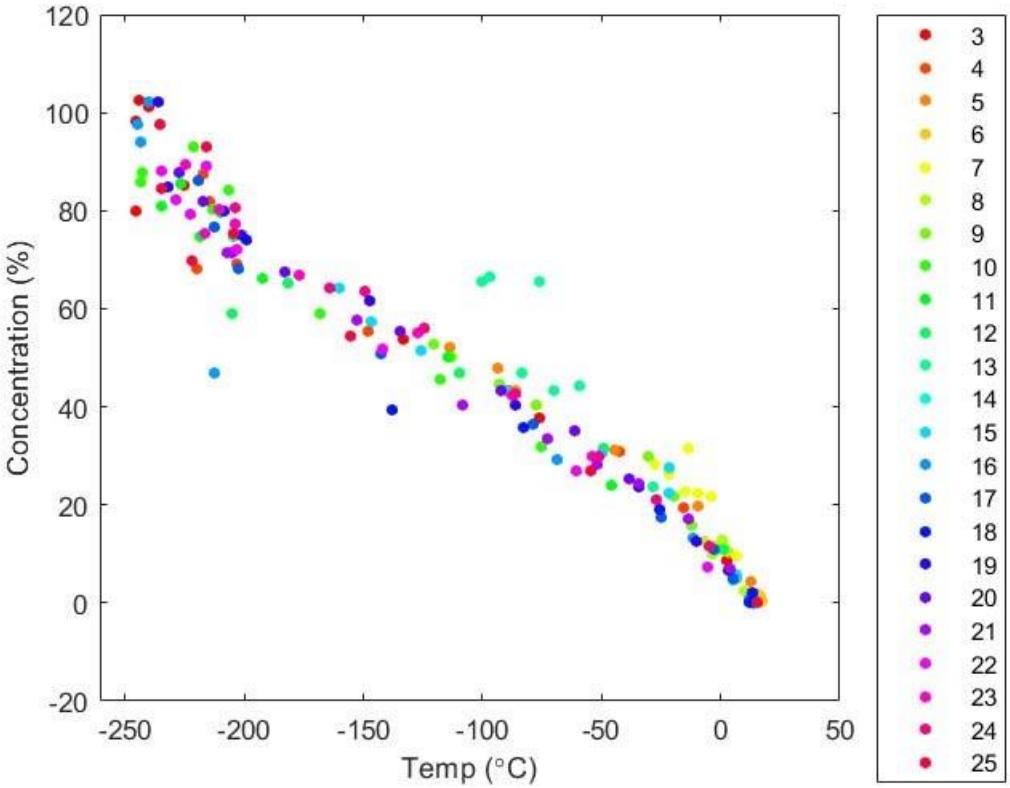

Figure 45: Graph showing the minimum measured temperature and maximum measured near-field concentrations at points along the centreline coloured by trial.

The H_2 sensors in the far-field had a response time of approximately 20 s. This means that the raw data will not show the concentration of transient pockets of H_2 without extrapolation. What can be directly obtained, however, is whether the H_2 concentration sensor over-ranged, which occurs at H_2 concentrations above 4%.

Table 15 shows over-ranging and estimated maximum average concentrations of transient H_2 pockets at a distance of 14 m from the release point 1.5 m height, which is the sensor location furthest from the release point along the centerline. The estimation is derived from an extrapolation of the peak value of the sensors in relation to the response time. The table shows the releases from 0.5 m height for a comparison of the effect of different pressures and nozzle sizes. The estimated maximum values for the 6 mm tests are extrapolated from the raw data by averaging the concentration of a transient H_2 pocket.

Table 15: Estimated maximum H_2 concentration.

Trial No.	Nozzle size	Pressure (Bar)	Distance (m)	Height (m)	Sensor overrange	Estimated max (%)
3	25.4 mm	1	14	1.5	Yes	> 4%
4	12 mm	1	14	1.5	Yes	> 4%
5	6 mm	1	14	1.5	No	2.15
10	25.4 mm	5	14	1.5	Yes	> 4%
11	12 mm	5	14	1.5	Yes	> 4%
12	6 mm	5	14	1.5	No	3.32

With regard to wind conditions the release direction was approximately 75°, meaning that a wind direction of 255° would be co-flow. The weather station in the far-field, that logged at 1 Hz, experienced a fault on trials 16-23. Five-minute average readings were taken with the local station for these tests. Figure 46 and 47 are example wind roses from trial 5 and 10 respectively. More details are provided with the detailed data on KITOpen repository.

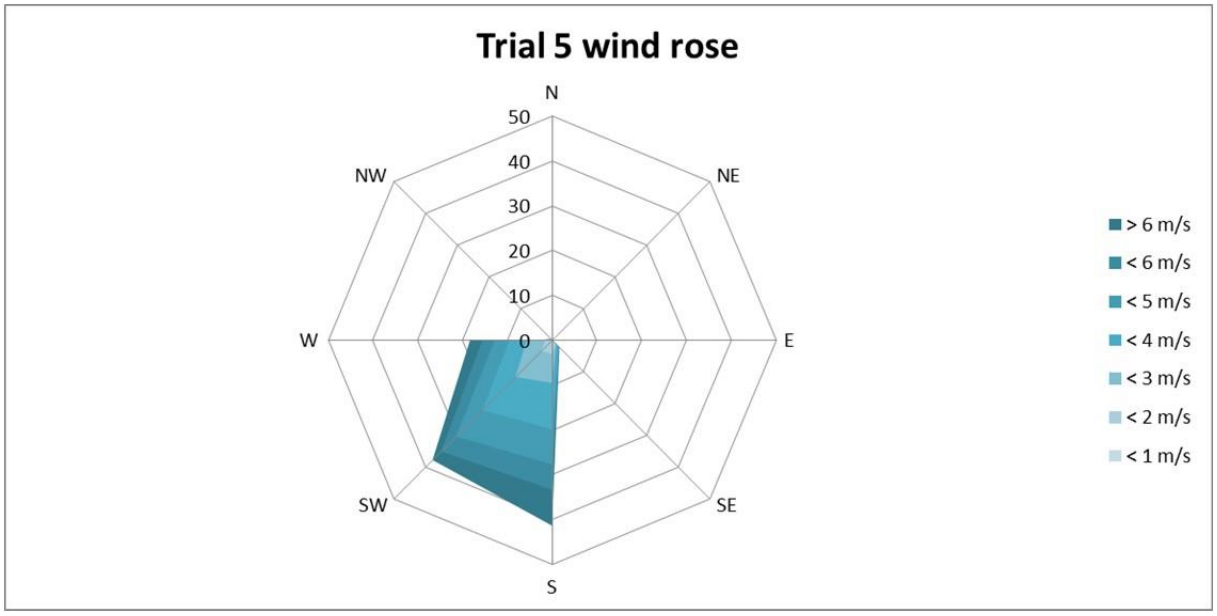

Figure 46: Wind rose showing wind direction, speed and proportion for trial 5.

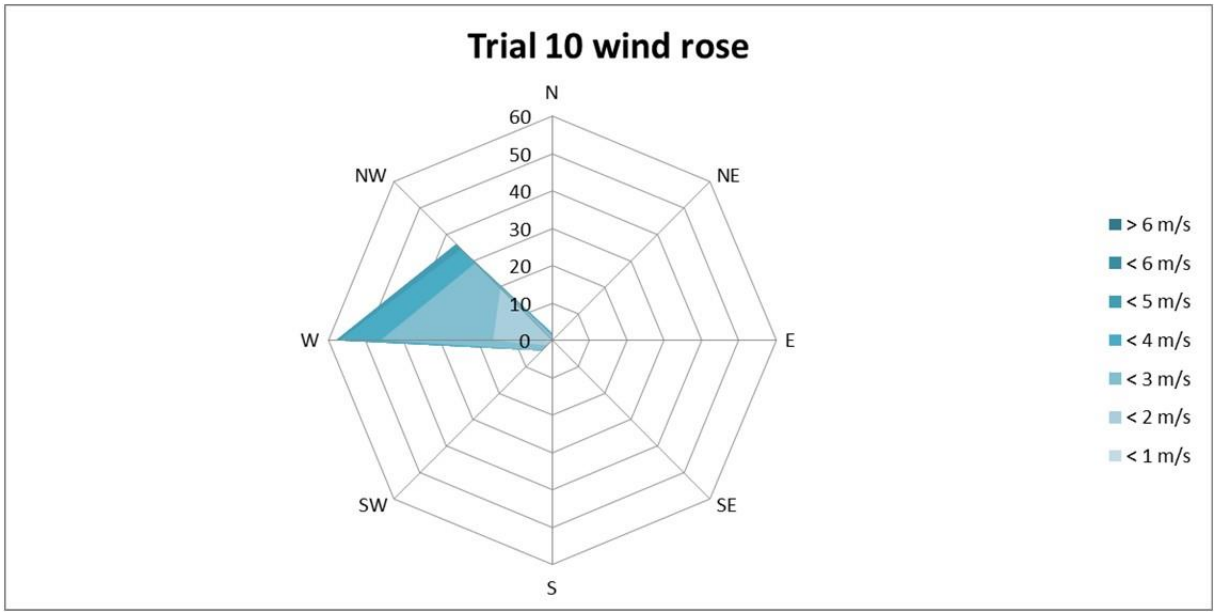

Figure 47: Wind rose showing wind direction, speed and proportion for trial 10.

6 Summary, Conclusions and Outlook

In the frame of the PRESLHY work package WP3 a broad set of experiments were performed to improved the understanding of release and mixing phenomena relevant in potential accidents with cryogenic or liquid hydrogen.

With more about 250 hydrogen blow-down experiments with the DISCHA and CRYOSTAT facility of KIT the flashing multiphase, multicomponent release phenomena and the free cryogenic jet principle structure was studied down to 20 K and up to 20 MPa. From these experiments inventory, pressure, and orifice diameter dependent characteristics like the discharge coefficient can be derived, which are necessary for defining hazard distances or may be used in other correlations for risk assessment in general. The influence of heat transfer and non-equilibrium states were checked. Moreover these tests provided the reference data for the transient jet fire experiments executed in work package WP4.

The POOL experiments provided useful insights in the heat transfer into LH2 pools for varying ground substrates and side wind conditions. Correlations for boiling heat transfer models could be validated and evaporation rates under different initial temperature conditions were provided.

The rain-out experiments performed by HSE demonstrated that rain out and pool formation will only occur for massive releases pointing downwards to the ground. The exterior mixing process provided an almost perfect inverse correlation of temperature and hydrogen concentration, what might support detection by simple temperature sensors in the vicinity of LH2 pipes or storages.

In none of the many release and mixing processes spontaneous ignition was observed. The induced electric fields and currents are obviously too small, although for cryogenic conditions the formation of ice, which is then entrained in the released gases, might yield considerable electrical fields.

Still open is the determination of the components of the ice, forming on the release nozzles or in a pool of larger releases. Also the multiphase effects on large scale dispersion with obstruction and/or (partial) confinement should be studied more intensively, as they might play a crucial role in maritime applications of LH2.

The improved knowledge of release and mixing should be used to assess more application oriented problems. For instance, the design and approval of safety valves and rupture membranes for LH2 cryostats could benefit from the deepened insights. In general, mitigation technology and strategies, including ventilation, water spray and sensor design and operational strategies (including placement) should assessed for proper hazard and risk assessment and safety management especially for scenarios in partially or fully closed rooms.

7 References

[1] KITopen, public research data repository; link for datasets and this report: https://doi.org/10.5445/IR/1000096833

[2] McCarty, R.D., Hord, J., and Roder, H.M.; Selected properties of hydrogen (engineering design data). Final report. United States: N. p., 1981. Web.

[3] V.K. Dhir; Boiling Heat Transfer, Ann. Rev. Fluid Mech. 1998, Vol 30, p. 365-401

[4] Y. Shirai et al, Boiling heat transfer from a horizontal flat plate in a pool of liquid hydrogen, Cryogenics 50 (2010) 410-416

[5] M. Kida et al, Pool-Boiling Heat Transfer in Liquid Nitrogen, J. Nuclear Science and Technology 18(7), July 1981